Deep–Sea Research I 190 (2022) 103899

Contents lists available at ScienceDirect

Deep-Sea Research Part I

journal homepage: www.elsevier.com/locate/dsri

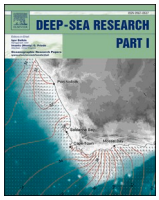

# Distribution and export of particulate organic carbon in East Antarctic coastal polynyas

Lavenia Ratnarajah [a,b,*], Viena Puigcorbé [c,d,**], Sébastien Moreau [e,f,g], Montserrat Roca-Martí [h,i], Julie Janssens [g], Matthew Corkill [g], Luis Duprat [f,g], Cristina Genovese [f,g], Jan Lieser [g,j], Pere Masqué [d,k], Delphine Lannuzel [g]

[a] Antarctic Climate and Ecosystems Cooperative Research Centre, University of Tasmania, Hobart, Tasmania, Australia
[b] Department of Earth, Ocean and Ecological Sciences, School of Environmental Sciences, University of Liverpool, UK
[c] Department of Marine Biology and Oceanography, Institut de Ciències del Mar (ICM-CSIC), Barcelona, Spain
[d] Centre for Marine Ecosystems Research, School of Science, Edith Cowan University, Joondalup, WA, Australia
[e] Norwegian Polar Institute, Fram Centre, PO Box 6606 Langnes, NO-9296, Tromsø, Norway
[f] Australian Research Council Antarctic Gateway Partnership, University of Tasmania, Hobart, Tas, Australia
[g] Institute for Marine and Antarctic Studies, University of Tasmania, Hobart, Tas, Australia
[h] Department of Oceanography, Dalhousie University, Halifax, Nova Scotia, Canada
[i] Department of Marine Chemistry and Geochemistry, Woods Hole Oceanographic Institution, Woods Hole, MA, USA
[j] Bureau of Meteorology, Hobart, Tasmania, Australia
[k] International Atomic Energy Agency, Principality of Monaco, Monaco

ARTICLE INFO

*Keywords:*
Particulate organic carbon
POC export
$^{234}$Th
Polynya
Southern ocean
East Antarctica

ABSTRACT

Polynyas represent regions of enhanced primary production because of the low, or absent, sea-ice cover coupled with the proximity of nutrient sources. However, studies throughout the Southern Ocean suggest elevated primary production does not necessarily result in increased carbon export. Three coastal polynyas in East Antarctica and an off-shelf region were visited during the austral summer from December 2016 to January 2017 to examine the vertical distribution and concentration of particulate organic carbon (POC). Carbon export was also examined using thorium-234 ($^{234}$Th) as a proxy at two of the polynyas. Our results show that concentrations and integrated POC stocks were higher within the polynyas compared to the off-shelf sites. Within the polynyas, vertical POC concentrations were higher in the Mertz and Ninnis polynyas compared to the Dalton polynya. Similarly, higher carbon export was measured in the diatom-dominated Mertz polynya, where large particles (>53 μm) represented a significant fraction of the particulate $^{234}$Th and POC (average 50% and 39%, respectively), compared to the small flagellate-dominated Dalton polynya, where almost all the particulate $^{234}$Th and POC were found in the smaller size fraction (1–53 μm). The POC to Chlorophyll-a ratios suggest that organic matter below the mixed layer in the polynyas consisted largely of fresh phytoplankton at this time of the year. In combination with a parallel study on phytoplankton production at these sites, we find that increased primary production at these polynyas does lead to greater concentrations and export of POC and a higher POC export efficiency.

## 1. Introduction

The biological carbon pump plays an important role in the removal of atmospheric carbon dioxide (Marinov et al., 2006). The photosynthetic production of particulate organic carbon (POC) by marine phytoplankton can globally transfer an estimated 10 Pg of carbon from the euphotic zone into the ocean interior each year (Falkowski et al., 1998; Passow and Carlson 2012). In large areas of the Southern Ocean, phytoplankton growth is regulated by the scarcity of iron (Martin 1990; Boyd et al., 2017), and seasonal co-limitation by light (Mitchell et al.,

*Abbreviations:* POC, Particulate Organic Carbon; $^{234}$Th, Thorium-234.

* Corresponding author. Antarctic Climate and Ecosystems Cooperative Research Centre, University of Tasmania, Hobart, Tasmania, Australia.
** Corresponding author. Department of Marine Biology and Oceanography, Institut de Ciències del Mar (ICM-CSIC), Barcelona, Spain.
*E-mail addresses:* Lavenia.Ratnarajah@utas.edu.au (L. Ratnarajah), Viena.Puigcorbe@outlook.com (V. Puigcorbé).

https://doi.org/10.1016/j.dsr.2022.103899
Received 7 April 2022; Received in revised form 10 October 2022; Accepted 12 October 2022
Available online 21 October 2022

1991; Strzepek et al., 2012) due to the deep mixed layer and ice cover that are prevalent in early spring, autumn, and winter which limits the efficiency of the biological carbon pump. However, the austral spring-time melting of sea ice (Sedwick and Di Tullio 1997; Lannuzel et al., 2011), ice shelves (Herraiz-Borreguero et al., 2016), and icebergs (Lin et al., 2011), coupled with pelagic recycling (Boyd et al., 2017; Ratnarajah et al., 2018), and the resuspension of shelf sediments (Sedwick et al., 2008; McGillicuddy et al., 2015) represent important sources of iron in these high-latitude iron-limited systems, which fuel phytoplankton primary production.

In the Southern Ocean, near the Antarctic coast, sea ice is typically drifting with the Antarctic Coastal Current westward around the continent. Grounded icebergs and coastal promontories create barriers to this drift. Upstream of these barriers, sea ice accumulates and becomes fastened, while downstream, open water areas known as latent heat polynyas are maintained via katabatic winds and ocean currents that transport new ice offshore (Andersen 1993). These latent heat polynyas are acknowledged as 'sea-ice factories' due to the rapid sea-ice formation and export from the strong and persistent katabatic winds (Fraser et al., 2012). Owing to their low or absent sea-ice cover, and proximity to iron sources, coastal polynyas are characterized by intense phytoplankton blooms which account for up to 65% of total production on the Antarctic continental shelf (Arrigo and van Dijken 2003; Alderkamp et al., 2012a; Gerringa et al., 2012). The increased phytoplankton production supports a thriving food web from microbes to higher trophic level organisms (Karnovsky et al., 2007; Ducklow et al., 2015; Yager et al., 2016). However, the timing, extent and intensity of primary production vary considerably amongst Antarctic polynyas. Satellite derived annual primary production estimates range from 18 ± 24 g C $m^{-2}$ in the Lützow-Holm Bay polynya to 161 ± 37 g C $m^{-2}$ in the Amundsen Sea polynya, with peak phytoplankton blooms occurring between December and February, depending on the polynya (Arrigo and van Dijken 2003; Arrigo et al., 2015; Liniger et al., 2020).

POC export from surface water to depth provides a mechanism for storing carbon in the deep ocean, however elevated primary production does not necessarily lead to increased carbon export. Studies have shown an increase in carbon flux with primary production due to passive sinking of organic particles (e.g., phytodetritus, resting spores, zooplankton fecal pellets, enhanced aggregates due to transparent exopolymer particles production) (Steinberg and Landry 2017; Rembauville et al., 2015), physical mixing via the mixed layer pump (Dall'Olmo et al., 2016), and active transport via zooplankton vertical migration (Turner 2015; Steinberg and Landry, 2017; Behrenfeld et al., 2019). In contrast, others demonstrated an inverse relationship between ocean primary production and export efficiency (export/net primary production (NPP)) of POC that was attributed to a combination of rapid microbial recycling, export of dissolved organic carbon, and grazer-mediated export (Maiti et al., 2013; Ducklow et al., 2015; Le Moigne et al. 2016; Lee et al., 2017; Henson et al., 2019) or by a long-time lag (e.g. 20–30 days, Henson et al., 2015) between the production and export of organic particles from the euphotic zone (Stange et al., 2017; Puigcorbé et al., 2017a; Laws and Maiti 2019). With increasing temperatures, the phytoplankton community could shift towards smaller sized cells (Montes-Hugo et al., 2009; Deppeler and Davidson 2017, Tréguer et al. 2017), but whilst export efficiency may decrease due to more organic carbon remineralization in the upper ocean, changes in export production are unclear (Fan et al., 2020).

As evidenced above, POC is a highly dynamic carbon pool and its variability is not well constrained due to different rates and pathways driven by local dynamics. In a parallel study to this, Moreau et al. (2019) measured high net community production (up to 75 mmol C $m^{-2}$ $d^{-1}$) within three coastal polynyas in East Antarctica (the Dalton, Mertz and Ninnis polynyas). Quantifying the links between surface production and POC distribution and export through the water column is key to evaluating the potential of these highly productive Antarctic coastal polynyas to export carbon now and in the future. The East Antarctic Southern Ocean is historically under studied, both spatially and seasonally, even more if we are looking into coastal areas (Hoppema and Anderson, 2007). In this study, we examine the vertical distribution of POC in these three coastal polynyas, as well as an off-shelf region for comparison, together with POC to chlorophyll-a (Chl-a) ratios, POC to particulate nitrogen (POC:PON, later referred to as C:N) ratios and ammonium concentrations, which were used as indicators of autotrophic and heterotrophic processes. Export fluxes of POC were also obtained using thorium-234 ($^{234}$Th, half-life = 24.1 days) in the Dalton and Mertz polynyas to elucidate the key drivers behind the POC distribution in these coastal polynyas.

## 2. Methods

### 2.1. Site description

The sampling sites of this study are located in latent heat polynyas, west of the Dalton Iceberg Tongue (Dalton Polynya), west of the Mertz Glacier Tongue (Mertz Polynya) which was significantly shortened in 2010 (Giles 2017), and west of the Ninnis Ice Shelf (Ninnis Polynya) (Fig. 1). The three polynyas are located on the East Antarctic coastal shelf. A detailed description of the physical oceanography of these polynyas can be found in Silvano et al. (2017). It is worth noticing, that inputs of modified Circumpolar Deep Water (mCDW) were different among the three polynyas, with shallow mCDW present in the Mertz and Ninnis polynyas due to a dense layer of high-salinity shelf waters (HSSW) compared to the Dalton polynya, where no HSSW was observed and the mCDW was found at depth (Silvano et al., 2017) which impacted the productivity of these polynyas (Moreau et al., 2019).

The Dalton polynya opened in September/October 2016, having the beginning of the bloom in mid-November, and remaining ice-free during December and January. This polynya was sampled between 30 December 2016 and 2 January 2017. In the Mertz and Ninnis polynyas the ice-free period started later, and the beginning of the bloom took place in late-November/early-December 2016. The Mertz and Ninnis polynyas were sampled between 9–13 January 2017. The ice conditions were a bit more dynamic in this region than in the Dalton polynya, with more sea-ice floating freely with the winds and currents. In general terms, the sea-ice encountered during sampling in late December-early January 2016/17 was in an advanced stage of melting following a peak phytoplankton bloom and was considered typical for this time of year. Off-shelf stations (ice-free) were also sampled during this study along the World Ocean Circulation Experiment (WOCE) SR3 repeat hydrographic line, between Tasmania and Antarctica. Measurements were taken south of the Polar Front, between 61.8°S and 67.9°S along the 140°E meridian.

A total of 71 CTD (conductivity-temperature-depth, SeaBird 704, SeaBird Inc., Bellevue, USA) casts were deployed within the Dalton (n = 19), Mertz (n = 24) and Ninnis (n = 14) polynyas, and in the off-shelf region (n = 14) moving away from the coastal polynyas (Fig. 1). Of these, 9 CTDs in the Dalton, 14 in the Mertz, 12 in the Ninnis, and 2 in the off-shelf region were sampled for *in situ* POC and PON measurements (yellow circles, Fig. 1). A total of 8 stations (4 in the Dalton and 4 in the Mertz polynyas) were also sampled for $^{234}$Th (black dots, Fig. 1).

### 2.2. Depth categories

The euphotic depth was considered as the depth at which photosynthetic available radiation (PAR) falls to 0.1% of its surface incident value. There are various methods to calculate mixed layer depths. Melting sea ice would influence the salinity, and consequently the density gradient. Therefore, we used the sea surface density at 10 m as in de Boyer Montégut et al. (2004) and determined the depth of the upper mixed layer using the commonly applied threshold of 0.01 kg $m^{-3}$ density increase relative to the sea surface density at 10 m (Thomson and Fine, 2003). To estimate $^{234}$Th fluxes (see section 3.5), we used the

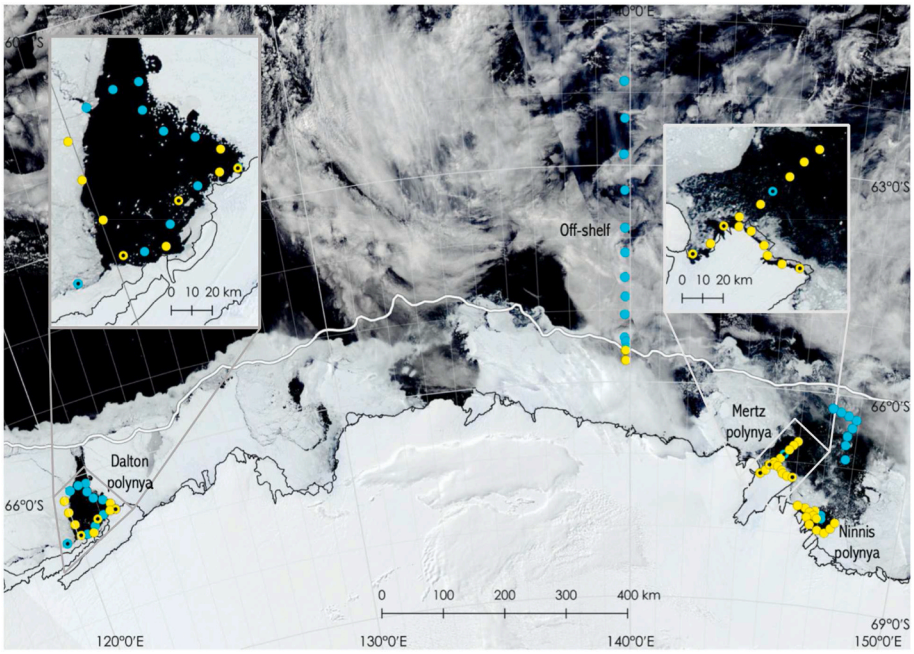


**Fig. 1.** Station location for the Dalton, Mertz and Ninnis polynyas, and the off-shelf region. Yellow dots denote sites where discrete particulate organic carbon measurements were taken. Blue dots represent sites where particulate organic carbon was extrapolated based on measurements of particulate beam attenuation coefficient at 660 nm. Smaller black dots represent where thorium-234 samples were taken. The thick white line indicates the shelf break. Background image from NASA Worldview (https://worldview.earthdata.nasa.gov; 12 January 2017). Smaller boxes highlight the sampling strategy within the Dalton and Mertz polynyas in greater detail as there were many stations in relatively close proximity, and thus difficult to discern where thorium-234 samples were taken alongside discrete and extrapolated particulate organic carbon measurements.

following depth horizons in addition to the euphotic depth: the depth where the shallow *in situ* pumps were deployed (section 2.6); the equilibrium depth (Eq depth), which is the shallowest depth where $^{234}$Th and $^{238}$U are in equilibrium; and the primary production zone (PPZ) which is defined as the first depth below the fluorescence peak where fluorescence is 10% of its maximum value in the water column (Owens et al., 2015).

### 2.3. Particulate organic matter concentration using Niskin bottles

Seawater samples were collected from Niskin bottles triggered at various depths during the CTD casts. Between 4 and 6 depths (10–200 m) were sampled for POC and PON based on the CTD PAR and Chl-a profiles (Moreau et al., 2019). Seawater samples were filtered (475–1, 055 mL depending on organic matter content) onto pre-combusted (450°C for 12 h), 25 mm, quartz fiber filters (Advantec). All glassware in contact with POC samples were also pre-combusted prior to the voyage and subsequently rinsed with 2% v/v hydrochloric acid and ultra-high purity water between samples. Filters were then removed and placed into individual, sterile filter holders and wrapped in pre-combusted aluminum foil to limit light exposure. Filters were stored at −20°C until analysis (~6 months). Nine unused, pre-combusted filters were analyzed as 'filter blanks' to quantify background concentration of POC and PON on the filters.

POC and PON were determined using standard carbon-hydrogen-nitrogen combustion methods (Knap et al., 1994). Filters were removed from storage, punched to 15.9 mm diameter, and dried in an oven at 60°C overnight in muffled glass trays. 80 μL of 10% v/v hydrochloric acid was then added to each filter to remove any inorganic carbon. The acid-treated filters were subsequently dried in a desiccator overnight, folded and enclosed into 8 × 5 mm silver capsules (Elemental Microanalysis, UK) and analyzed at the Central Science Laboratory, University of Tasmania, using a Thermo Finnigan EA 1112 Series Flash Elemental Analyzer (estimated precision ~ 1%). The final POC and PON concentrations were calculated by subtracting the average carbon and nitrogen content measured in the filter blanks (3 ± 1 μg for carbon and 0.3 ± 0.1 μg for nitrogen), multiplying by the filter to punch area ratio and dividing the values by the volumes filtered. POC and PON measurements were not corrected for possible dissolved organic carbon and nitrogen adsorption on the filters.

### 2.4. POC and particulate beam attenuation coefficient

The determination of POC concentration from discrete bottle samples within a dense spatial grid is time and labor intensive. Therefore, we estimated the POC distribution along the water column by relating the discrete POC concentration to the 660 nm wavelength measurements obtained with an *in situ* optical instrument (Wetlabs C-star transmissometer serial no. 1421DR 25 cm pathlength). This method has been demonstrated to successfully examine the spatial and vertical distribution of POC in the past (e.g., Bishop 1999, Mishonov et al., 2003, Gardner et al., 2018a, b). The upcast transmissometer profile of the water column was used as it paired with the firing of the Niskin bottles for subsequent POC analysis in water samples. Upcast profiles were not affected by bottle firing (Supplementary Fig. 1). Baseline data were vertically averaged in 2 dbar (~2 m) bins. Factory calibration details are presented in Rosenberg and Rintoul (2017). The optical sensor output was delivered in percent units. The percent transmission (Tr) of light was then converted to total beam attenuation coefficients ($c$) using:

$$c = -(1 / r) * \ln (Tr / 100)$$

where $c$ = beam attenuation coefficient ($m^{-1}$), r = beam path length (0.25 m), and Tr = beam transmission (%) (Gardner et al., 1995). The beam attenuation coefficient represents the sum of attenuation due to particles ($c_p$), seawater ($c_{sw}$) and colored dissolved organic matter (CDOM). Scattering and absorption by CDOM is considered negligible in most open ocean waters including the Southern Ocean, so attenuation by particles ($c_p$) equals the total attenuation measured (c) minus the attenuation by water ($c_{sw}$):

$$c_p = c - c_{sw}$$

where $c_{sw}$ was derived from measurements of $c$ at 2,000 m depth at the off-shelf sites (depths were above the nepheloid layer), where particle concentrations can be assumed to be negligible. A 5-point running median followed by a 7-point running mean was applied as a low-pass filter (Briggs et al., 2011).

The POC:$c_p$ relationship was assessed based on sites where POC and $c_p$ were simultaneously determined. Particulate attenuation, $c_p$, was linearly correlated with discrete POC concentration (with a coefficient of determination of $R^2 = 0.76$). There was no evidence of site differences

between the *in situ* POC concentration and particulate attenuation ($p = 0.4$), which allowed for the POC concentrations to be pooled across all CTDs for each polynya, and the off-shelf stations (Fig. 2). $c_p$ was transformed to POC concentration (mg $m^{-3}$) via a single linear equation:

$$POC = 17.3 + 383.6c_p$$

### 2.5. Total $^{234}Th$ and $^{238}U$ activities in seawater

Seawater samples (4 L each) were collected along the water column (between 6 and 16 depths down to 230–800 m). After collection, samples were acidified to pH < 2 with nitric acid and spiked with a known amount of $^{230}Th$ and were processed using the manganese oxide co-precipitation technique (Benitez-Nelson et al., 2001; Clevenger et al., 2021). A gas flow low-level background beta counter was used on board to conduct the first counting (counting statistics <3%) (RISØ, Denmark). Samples were recounted 6 months later to determine background activities. After the second counting, samples were processed following the method described in Puigcorbé et al. (2017a) to determine the potential losses of thorium during sample processing. $^{230}Th$:$^{229}Th$ ratios were measured using ICP-MS at the Alfred Wegener Institute (Germany) with an average recovery of 91 ± 9% (n = 107). $^{238}U$ activities (in dpm $L^{-1}$) were determined from salinity data using the relationship from Owens et al. (2011). Calibration for the efficiency of the detectors was carried out using $^{238}U$ standards and deep-water samples (2,000–2,900 m) were used to confirm the calibration.

### 2.6. Particulate $^{234}Th$ and POC using in situ pumps

Size-fractionated particles for the measurement of $^{234}Th$ and POC were collected using *in situ* pumps (ISP; McLane) from a total of 8 casts. Depending on the water column depth, one or two ISP were deployed at 100–160 m (hereafter shallow ISP) and 300 m (hereafter deep ISP). The pumping time varied between 1.5 and 2 h, allowing a total filtration volume of 250–420 L. The ISP were equipped with 142 mm diameter filter holders containing two filter types, a Nitex screen (53 μm) followed by a quartz filter (QMA, Millipore, 1 μm), thus allowing for particle size fractionation: 1–53 μm and >53 μm. All filters were acid cleaned and QMAs were combusted prior to sampling.

Particulate material collected on the Nitex screens (>53 μm) was rinsed using filtered seawater (<0.2 μm), collected in an acid-cleaned plastic beaker and stirred to homogenize the sample. A volumetric fraction of the rinsed solution, representing 30–80% of the total volume, was filtered onto a pre-combusted 25 mm QMA filter for $^{234}Th$ and POC analyses. For $^{234}Th$ and POC analyses in QMAs (1–53 μm), a 25 mm punch was used to subsample 3 replicates from each filter. All filters were then dried overnight at 50 °C, counted for $^{234}Th$ at sea and recounted for background activities 6 months later, as was done for the seawater samples. After the background counting, samples were treated to analyze POC by adding hydrochloric acid to remove inorganic carbon and then measured by high temperature combustion using a Costech Elemental Analyzer. POC concentrations were calculated by subtracting the average carbon measured in dipped filter blanks before dividing by the filtered volume. Blanks for POC (5.3 ± 0.6 μg/filter, n = 3) were obtained from dipped filters and represented, on average, 1.8 ± 1.0% of the total amount measured in the samples from both size fractions (n = 56). POC and $^{234}Th$ measurements in triplicate QMA punches showed a relative standard deviation of 4.1 ± 2.5% and 7.6 ± 3.5%, respectively.

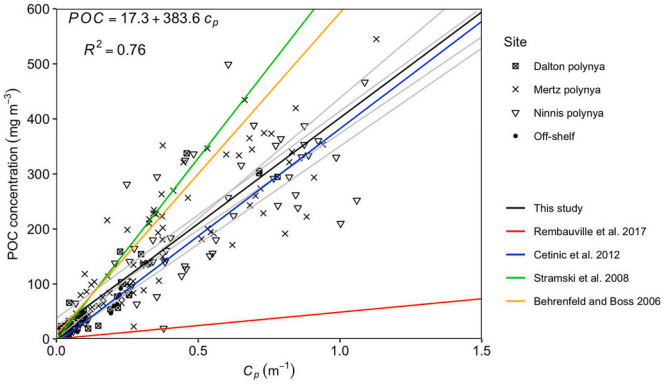


**Fig. 2.** Relationship between *in situ* particulate organic carbon (POC) concentration (mg $m^{-3}$) and particulate beam attenuation coefficient ($c_p$, $m^{-1}$). Grey lines indicate the slope for each site. We found no evidence of site differences ($p = 0.1$); therefore, one common line (black line) fits all sites. Overlaid in red (Rembauville et al., 2017), blue (Cetinić et al., 2012), green (Stramski et al., 2008), and orange (Behrenfeld and Boss, 2006) are the relationships reported by previous studies for comparison.

### 2.7. Ammonium in seawater

Samples from each CTD were collected at 12 depths distributed between the surface and the bottom to determine the concentration of ammonium in seawater using a Seal AA3 HR Auto Analyzer based on the method by Kérouel and Aminot (1997). This method is based on the reaction of ammonium with ortho-phthaldialdehyde and sulfite at a pH of 9.0–9.5 producing an intensely fluorescent product; with an excitation at 370 nm, and emission at 460 nm. Interferences from amino acids present in the sample are eliminated by the specific combination of the working reagent. Salt effects are eliminated by keeping the Borax buffer at pH 9.0–9.5. Analysis was conducted at CSIRO, Hobart. The nominal method detection limit is 0.02 μmol $L^{-1}$. Method uncertainty at 1.0 μmol $L^{-1}$ is 0.066 μmol $L^{-1}$. Due to the unbalanced dataset along the vertical profiles, we used the nearest neighbor interpolation between data points for every 1 dbar interval, then averaged across all stations at every 5 dbar intervals to obtain the mean ammonium profile in the top 500 m.

### 2.8. Statistical analysis

A two-way ANOVA with interaction effect was used to determine if there was a significant difference in the relationship between POC and particulate beam attenuation coefficient by site (i.e., Dalton, Mertz, Ninnis, off-shelf). One-way ANOVA (Type I) was used to determine if POC concentration varied by site. A Type II ANOVA for unbalanced data was used to determine if there was a significant difference in ammonium concentration by site and C:N ratio by site and depth. Tukey HSD post hoc test was then conducted to examine the significance of differences between sites and depths and between the different depth horizons used to calculate the $^{234}Th$ export flux. All analyses were performed using R (R Core Team 2014).

## 3. Results

### 3.1. Euphotic and mixed layer depths

The median euphotic depths were found to be at 97 m, 40 m, 40 m and 118 m for the Dalton, Mertz and Ninnis polynyas, and the off-shelf region, respectively (Table 1). The mixed layer depths were consistently found to be shallower than the euphotic depths. Three sites in the southeast of the Dalton polynya had very deep mixed layer depths between 100 and 154 m. Excluding these sites the median mixed layer depths were 28 m, 12 m, 12 m, 17 m for the Dalton, Mertz and Ninnis polynyas, and the off-shelf region, respectively (Table 1).

### 3.2. POC profiles

POC concentrations decreased with depth in the Dalton polynya and

**Table 1**
Mixed layer depth, euphotic depth, particulate organic carbon (POC) concentration and integrated POC at various depths for the Dalton, Mertz and Ninnis polynyas, and the off-shelf sites. We report mean ± standard deviation, median and, Q1– Q3.

| Parameter | | Dalton polynya | Mertz polynya | Ninnis polynya | Off-shelf sites |
|---|---|---|---|---|---|
| Mixed layer depth (m) | mean ± sd | 43 ± 43 | 13 ± 1 | 13 ± 2 | 20 ± 7 |
| | median | 28 | 12 | 12 | 17 |
| | Q1– Q3 | 20–43 | 12–14 | 12–14 | 14–25 |
| Euphotic depth (m) | mean ± sd | 95 ± 56 | 13 ± 9 | 41 ± 6 | 113 ± 45 |
| | median | 97 | 40 | 40 | 118 |
| | Q1– Q3 | 45–135 | 34–46 | 39–44 | 79–138 |
| POC Within euphotic zone ($mg\ m^{-3}$) | mean ± sd | 59 ± 58 | 244 ± 71 | 275 ± 95 | 58 ± 27 |
| | median | 34 | 247 | 284 | 56 |
| | Q1– Q3 | 27–55 | 180–294 | 192–350 | 33–83 |
| POC Top 200 m ($mg\ m^{-3}$) | mean ± sd | 60 ± 62 | 121 ± 95 | 138 ± 124 | 47 ± 26 |
| | median | 32 | 81 | 77 | 34 |
| | Q1– Q3 | 26–65 | 48–177 | 35–224 | 27–59 |
| Integrated POC Top 200 m ($g\ m^{-2}$) | mean ± sd | 12 ± 7 | 23 ± 6 | 27 ± 6 | 9 ± 1 |
| | median | 8 | 23 | 28 | 9 |
| | Q1– Q3 | 7–18 | 20–27 | 24–30 | 8–10 |
| Integrated POC 200–500 m ($g\ m^{-2}$) | mean ± sd | 4 ± 3 | 7 ± 3 | 8 ± 1 | 6 ± 2 |
| | median | 3 | 8 | 8 | 7 |
| | Q1– Q3 | 1–7 | 5–10 | 8–9 | 5–8 |

at the off-shelf stations, while in the Mertz and Ninnis polynyas, POC increased and peaked at ~30 m depth prior to decreasing with depth (Figs. 3 and 4). Overall, the mean extrapolated POC profiles (black line) mostly tracked the station profiles (grey lines) but some degree of variability was observed (Fig. 4). In the upper 75 m of the Dalton polynya, three stations in the southeast of the polynya had much higher surface POC concentrations.

Within the euphotic zone, the highest derived POC concentrations were found in the Ninnis polynya (275 ± 95 mg $m^{-3}$, n = 256), followed by the Mertz (244 ± 71 mg $m^{-3}$, n = 2247) and Dalton (59 ± 58 mg $m^{-3}$, n = 1972) polynyas and lastly the off-shelf region (58 ± 27 mg $m^{-3}$, n = 1278; Table 1). There was a significant difference between the three polynyas ($p < 0.01$), but the Dalton polynya was not significantly different to the off-shelf region ($p = 0.9$). A similar pattern is observed when looking at the upper 200 m, where Ninnis (138 ± 124 mg $m^{-3}$) > Mertz (121 ± 95 mg $m^{-3}$) > Dalton (60 ± 62 mg $m^{-3}$) > off-shelf (47 ± 26 mg $m^{-3}$), although pairwise comparisons suggest that all 4 locations are significantly different to each other ($p < 0.01$) (Table 1). Optical spikes were evident at the bottom of some stations in the Mertz polynya (Fig. 4). As noted in the calibration report, the near bottom transmittance spikes are evident in the full 24 Hz data for some stations in the Mertz polynya (Rosenberg and Rintoul, 2017). Because these spikes are near the seafloor, they could be due to the presence of a nepheloid layer. The thickness of the nepheloid layer was calculated based on Gardner et al. (2018a,b) which is the distance between the $c_{Pmin}$ + 0.01 $m^{-1}$ and the profile bottom depth. In the Mertz polynya nepheloid layer thickness was 159 ± 163 m and removing the nepheloid layer would remove these spikes.

Because a large fraction of the POC pool is expected to be remineralized in the upper 200 m (Henson et al., 2012), depth integrated POC (Fig. 5) is presented for the top 200 m (Fig. 5a) and for 200–500 m, or to the maximum depth if shallower than 500 m (Fig. 5b). Moreover, the top 200 m layer matches the depth integrated Chl-a and net community production (NCP) estimates from a parallel study (Fig. 7 in Moreau et al., 2019). Depth integrated POC of the top 200 m was greatest in the Ninnis polynya (27 ± 6 g $m^{-2}$), followed by the Mertz polynya (23 ± 6 g $m^{-2}$), and were not significantly different to each other ($p = 0.1$), however they were significantly higher compared to the Dalton polynya and the off-shelf region ($p < 0.01$). The Dalton and the off-shelf region were not significantly different to each other ($p = 0.3$) with slightly higher integrated POC measured in the Dalton polynya (12 ± 7 g $m^{-2}$) compared to the off-shelf region (9 ± 1 g $m^{-2}$) (Fig. 5a; Table 1). The POC stocks between 200 and 500 m across all sites were significantly lower compared to the top 200 m (Fig. 5b). Integrated POC stocks between 200 and 500 m in the Ninnis and Mertz polynyas (8 ± 1 g $m^{-2}$ and 7 ± 3 g $m^{-2}$, respectively) were higher than the off-shelf region (6 ± 2 g $m^{-2}$). In the Dalton polynya, 13 out of the 19 sites had water column depths <500 m (between 230 and 322 m), thus integrated POC stocks were calculated from 200 m to seafloor at these sites (4 ± 3 g $m^{-2}$) and were found to be lower than the other polynyas and the off-shelf sites. Omitting these 13 sites where maximum depth was less than 500 m, depth integrated POC between 200 and 500 m for the remaining 6 sites increases to that observed for the Ninnis and Mertz polynyas (7 ± 1 g $m^{-2}$).

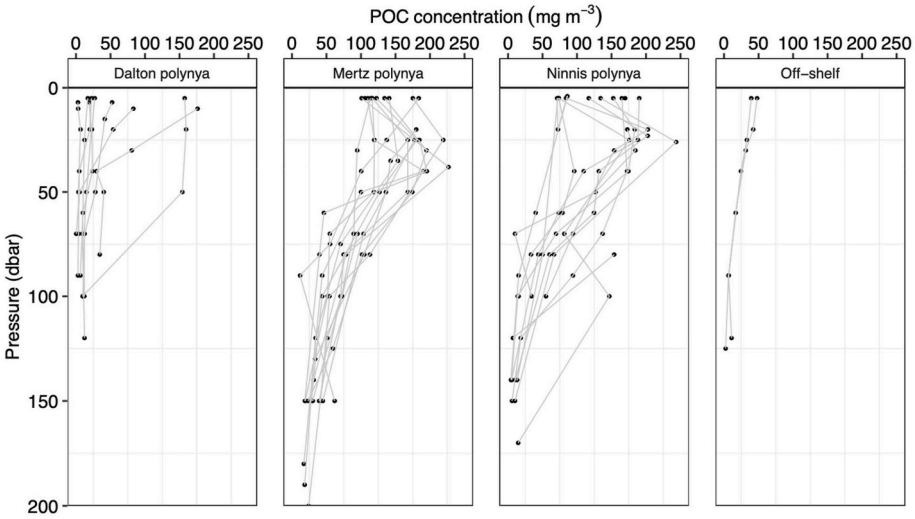


**Fig. 3.** Particulate organic carbon (POC) concentrations (mg $m^{-3}$) based on *in situ* measurements in the Dalton, Mertz, and Ninnis polynyas, and at the off-shelf stations.

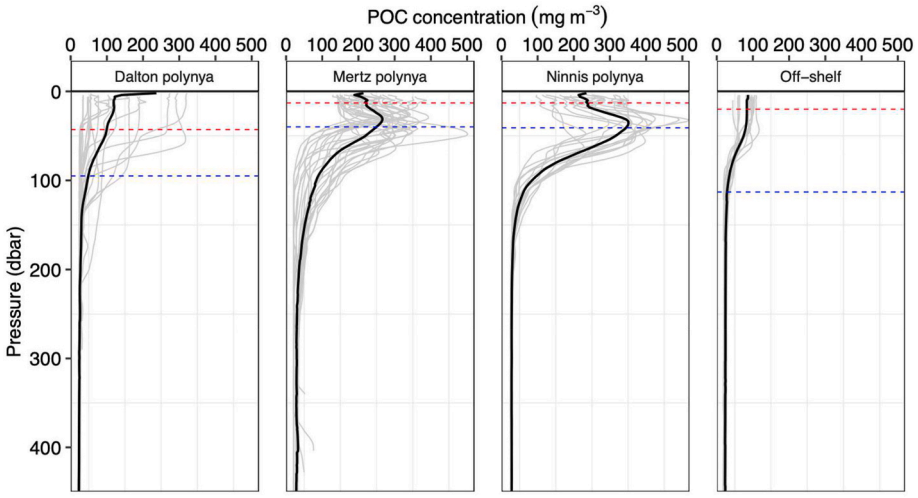


**Fig. 4.** Particulate organic carbon (POC) profiles extrapolated based on the linear regression between POC and $c_p$ (Fig. 2) across the entire water column for the Dalton, Mertz, and Ninnis polynyas, and the off-shelf sites. Grey lines represent individual station profiles, and the black line represents the mean profile. Red dashed horizontal line represents average mixed layer depth, whilst the blue dashed horizontal line represents the average euphotic depth.

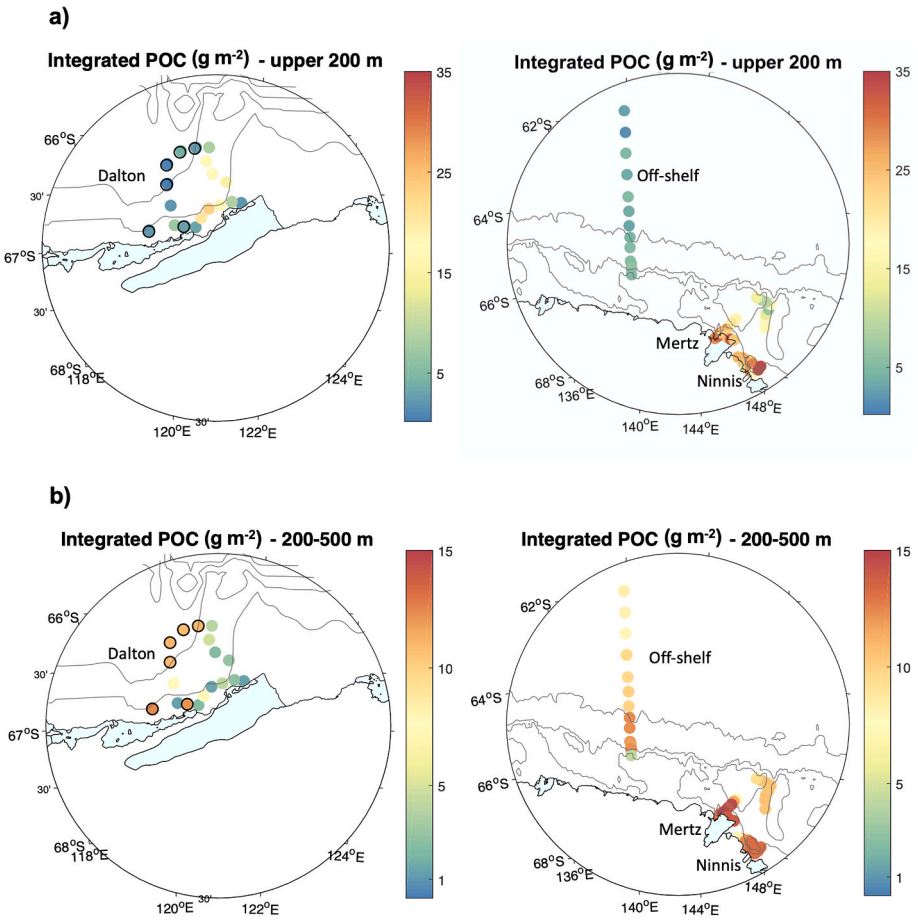


**Fig. 5.** Depth integrated particulate organic carbon (POC; g m$^{-2}$) in a) the top 200 m, and b) between 200 and 500 m (or bottom depth), for the Dalton, Mertz, and Ninnis polynyas, and the off-shelf sites. The black circles at the Dalton polynya denote those stations that reached 500 m (n = 6) the others (n = 13; the dot found in the most southeast location represents two stations) had depths between 230 and 322 m. Note the varying scales for POC stocks.

### 3.3. POC:Chl-a

The POC:Chl-a ratios were determined based on *in situ* sampling (Chl-a data from Moreau et al., 2019), consequently the ratios are only available for the upper 200 m. In general, the POC:Chl-a ratios were <200 mg mg$^{-1}$ and increased with depth (Fig. 6). POC:Chl-a ratio was >200 mg mg$^{-1}$ below 100 m at the off-shelf sites, and below ~150 m in the Dalton and Ninnis polynyas. The Mertz polynya was consistently <100 mg mg$^{-1}$ down to 200 m.

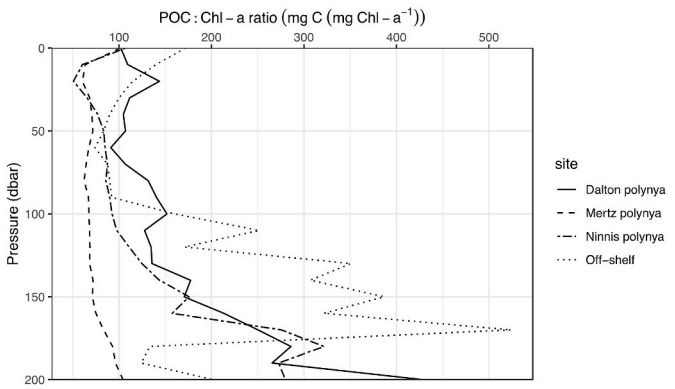


**Fig. 6.** Mean ratio of particulate organic carbon (POC) to chlorophyll-a (Chl-a) in the polynyas and off-shelf sites averaged every 10 dbar.

### 3.4. C:N ratio

The C:N ratios (calculated based on measured POC) in the Mertz polynya and the off-shelf sites were not significantly different to each other ($p = 0.1$). However, C:N ratios for all other site pairings were significantly different from each other ($p < 0.01$; Fig. 7). The C:N molar ratios were generally lower than the Redfield ratio of 6.6 in the upper 200 m (Fig. 7). In the Ninnis polynya, the C:N molar ratio averaged 5.7 ± 0.7 (n = 62), while it was 4.8 ± 0.9 (n = 73) in the Mertz polynya, 4.0 ± 0.6 (n = 11) at the off-shelf sites, and 2.8 ± 1.7 (n = 41) in the Dalton polynya (Fig. 7). Only the Dalton polynya showed a significant difference in C:N molar ratios with depth ($p < 0.01$). There were 7 instances (in blue, Fig. 7) where the blanks contributed to 31–46 % of the total carbon measured and C:N molar ratios were between 1.1 and 2.6. There were further 3 instances (in orange, Fig. 7) where the blanks contributed to 50–52 % of the total carbon measured and C:N molar ratios were between 0.8 and 0.9. Therefore, these measurements with a low signal to noise ratio should be taken with caution. At all other sites, C blank corrections were <30% of the total C measured for each sample (7.2% on average). There were no samples where the N blank correction was >30% of the total N measured (3.3% on average). Omitting the samples where C blank corrections were >30%, the mean C:N molar ratio in the Dalton polynya increased to 4.8 ± 1.2 and still showed a significant decrease in C:N molar ratios with depth ($p < 0.05$).

### 3.5. $^{234}$Th profiles and export fluxes

The Dalton and Mertz polynyas presented markedly different $^{234}$Th profiles. The Dalton polynya's $^{234}$Th activity concentrations in surface waters were relatively high (≥2 dpm L$^{-1}$) and equilibrium with $^{238}$U (2.4 dpm L$^{-1}$) was reached at depths no deeper than 100 m. In contrast, in the Mertz polynya, a clear deficit of $^{234}$Th with respect to $^{238}$U was present at all stations down to 70–125 m (Fig. 8), with $^{234}$Th:$^{238}$U activity ratios averaging 0.66 ± 0.15 (n = 17).

$^{234}$Th fluxes were obtained by integrating its deficit in the upper water column with respect to $^{238}$U, applying a 1D scavenging model assuming steady state conditions and considering there was no significant advection nor diffusion transport. The small $^{234}$Th deficits found in the Dalton polynya led to small (<800 dpm m$^{-2}$ d$^{-1}$) or even negligible $^{234}$Th export fluxes (Table 2). In contrast, the $^{234}$Th fluxes in the Mertz polynya were, on average, 5-fold higher than those measured in the Dalton polynya. The integration depth chosen can, in some cases, impact significantly the derived export flux. For that reason, we used four different depths horizons to calculate the $^{234}$Th fluxes: i) the depth where the shallow ISP were deployed; ii) the equilibrium depth (Eq depth); iii) the primary production zone (PPZ); and iv) the depth of the euphotic zone (Zeu) (see section 2.2; Table 2). Out of the four depths horizons chosen here, only the Zeu yielded significantly lower $^{234}$Th fluxes ($p < 0.001$), especially in the Mertz polynya, where $^{234}$Th deficits were found at depths below the Zeu resulting in significantly lower $^{234}$Th fluxes at this depth compared to the deeper depth horizons. There were no significantly different results ($p > 0.5$) among the other three integration depths, suggesting that PPZ, shallow ISP depth and Eq depth are a better definition of the base of the productive layer compared to Zeu in this study area. Therefore, since the goal is to estimate the export of POC out of the productive layer, we will consider the fluxes obtained at the shallow ISP depth where POC:$^{234}$Th ratios were measured (see Table 2 for ISP depth reference).

### 3.6. Particulate $^{234}$Th, POC and POC:$^{234}$Th ratios

In the Mertz polynya, the concentrations of particulate $^{234}$Th at the shallow ISP depths were >2 times higher compared to the Dalton polynya (0.321 ± 0.082 dpm L$^{-1}$ vs 0.140 ± 0.013 dpm L$^{-1}$), but particulate $^{234}$Th in the Dalton polynya was comparable to the concentrations measured at the deep ISP depth (300 m) in the Mertz (0.120 ± 0.013 dpm L$^{-1}$). The relative contribution of both particle sizes to particulate $^{234}$Th was also different between polynyas. At all the stations in the Dalton polynya, almost all of the particulate $^{234}$Th was measured in the small size fraction (98 ± 2%, Fig. 9). Comparatively, in the Mertz

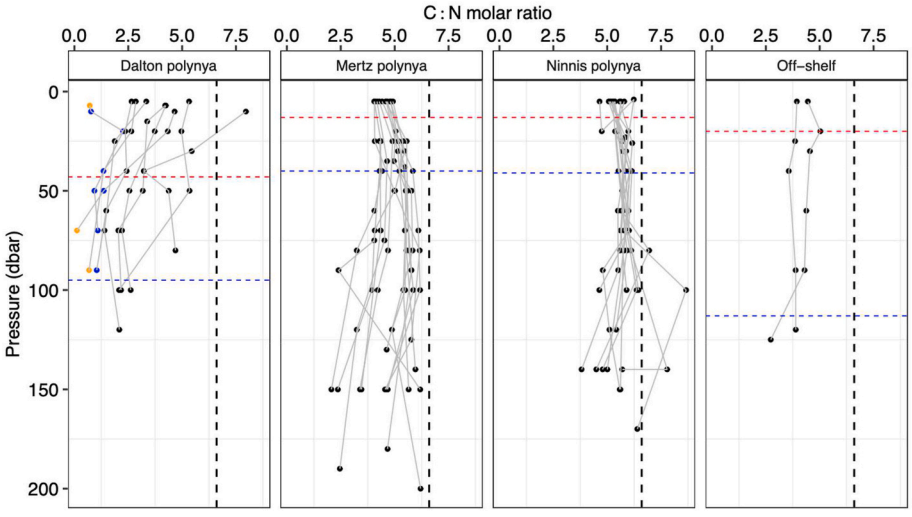


**Fig. 7.** Particulate organic carbon:nitrogen (C:N) molar ratios in the Dalton, Mertz, and Ninnis polynyas, and at the off-shelf sites. In the Dalton polynya, the blue points show samples where the blank contributed 31–46 % to C (n = 7), whilst the orange points show samples where the blank contributed 50–52 % (n = 3), and thus need to be taken with caution. Black dashed vertical line indicates the Redfield ratio (6.6). The blue and red dashed horizontal lines represent the average euphotic depth and the average mixed layer depth, respectively.

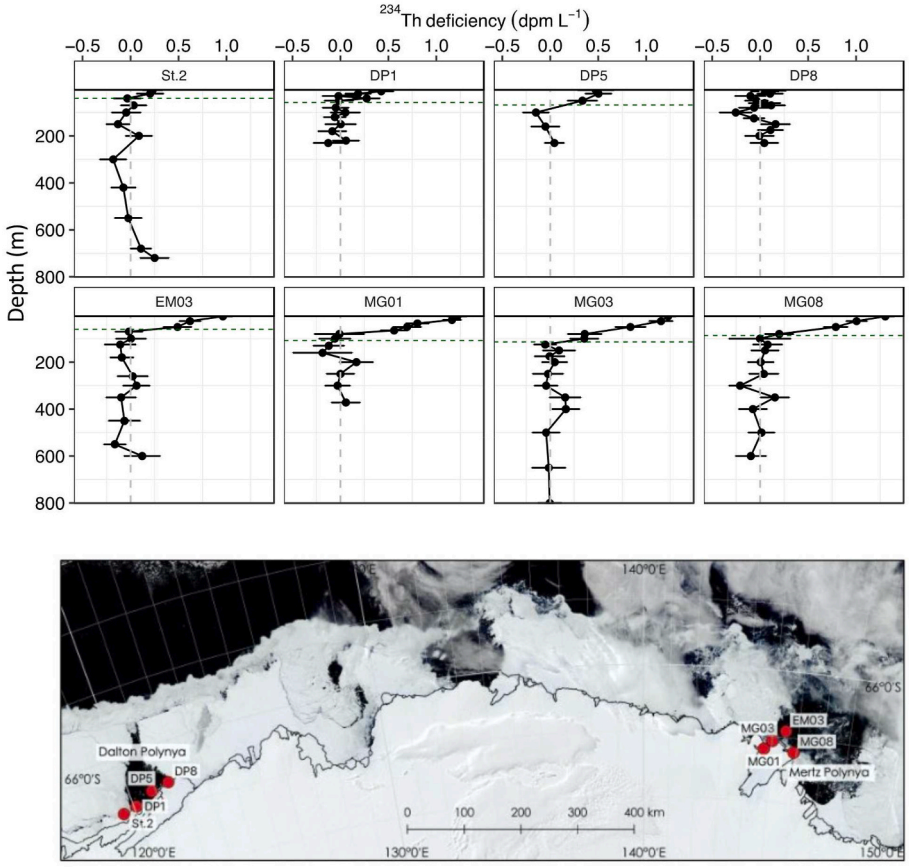


**Fig. 8.** Thorium-234 deficiency (black dots) concentration profiles along the water column at each station. The top four panels are stations located in the Dalton polynya and the lower four panels are stations sampled within the Mertz polynya. The dashed vertical grey lines indicate equilibrium. The green horizontal dashed lines show the depths at which fluorescence was 10% of its maximum signal in overlying waters (primary production zone, PPZ). The fluorescence profile was not available for station DP8. The map at the bottom shows the location of the stations sampled in each polynya.

**Table 2**
Thorium-234 ($^{234}$Th) fluxes estimated at several depth horizons: shallow *in situ* pump (ISP) depth, equilibrium depth (Eq depth), primary production zone (PPZ) and euphotic zone depth (Zeu). See section 2.2 for details. Particulate organic carbon (POC) fluxes at the depth of the shallow ISP are also provided.

| Polynya | Station | Shallow ISP depth | $^{234}$Th flux at shallow ISP depth | Eq depth | $^{234}$Th flux at Eq depth | PPZ depth | $^{234}$Th flux at PPZ depth | Zeu depth | $^{234}$Th flux at Zeu | POC fluxes at shallow ISP depth |
|---|---|---|---|---|---|---|---|---|---|---|
| | | (m) | (dpm m$^{-2}$ d$^{-1}$) | (m) | (dpm m$^{-2}$ d$^{-1}$) | (m) | (dpm m$^{-2}$ d$^{-1}$) | (m) | (dpm m$^{-2}$ d$^{-1}$) | (mmolC m$^{-2}$ d$^{-1}$) |
| **Dalton** | St. 2 | 100 | 167 ± 189 | 40 | 175 ± 91 | 40 | 175 ± 91 | 122 | 112 ± 214 | 1.2 ± 1.3 |
| | DP1 | 100 | 279 ± 168 | 30 | 234 ± 73 | 58 | | 74 | 284 ± 128 | 3.0 ± 1.8 |
| | DP5 | 160 | 600 ± 332 | 100 | 774 ± 236 | 68 | 689 ± 161 | 20 | 280 ± 75 | 6.0 ± 3.3 |
| | DP8 | 150 | −125 ± 205 | surface | – | ND | – | 170 | −48 ± 225 | – |
| **Mertz** | EM03 | 100 | 1122 ± 179 | 70 | 1127 ± 135 | 60 | 1059 ± 115 | 26 | 609 ± 56 | 9.3 ± 1.5 |
| | MG01 | 100 | 1805 ± 183 | 80 | 1824 ± 131 | 108 | 1784 ± 190 | 44 | 1306 ± 72 | 16.3 ± 1.7 |
| | MG03 | 100 | 2297 ± 206 | 125 | 2405 ± 228 | 114 | 2357 ± 216 | 46 | 1462 ± 96 | 24.7 ± 2.2 |
| | MG08 | 100 | 1977 ± 193 | 100 | 1977 ± 193 | 86 | 1938 ± 155 | 54 | 1552 ± 99 | 15.0 ± 1.5 |

ND = No data.

polynya the contribution of small particles to $^{234}$Th was found to be smaller and more variable across stations (63 ± 19%) with a minimum contribution of 40% (EM03 at 100 m, Fig. 9). In the Mertz polynya, we observed an increase of the percentage of $^{234}$Th in the small size fraction in the deep samples compared to the shallow samples (Fig. 9). The POC distribution between the two polynyas and between the size fractions mimics that of particulate $^{234}$Th. Almost the totality of POC was measured in the small size fraction in the Dalton polynya, whereas in the Mertz polynya the contribution of large particles to POC represented up to 42% of the POC (Fig. 9). POC and $^{234}$Th were found to correlate positively in the Mertz polynya when pooling all the data available ($R^2$ = 0.84, p = 0.00018, n = 14), but also when looking at the two size fractions separately (small particles: $R^2$ = 0.93, p = 0.0021, n = 7; large particles: $R^2$ = 0.88, p = 0.0082, n = 7). In the Dalton polynya, that relationship was only significant when pooling all the dataset ($\rho^2$ = 0.67, p = 0.029, n = 10).

The POC:$^{234}$Th ratios, multiplied by the flux of $^{234}$Th, are used to derive the POC fluxes. The shallow POC:$^{234}$Th ratios for small particles averaged 14 ± 9 μmol dpm$^{-1}$ in the Dalton polynya and 9 ± 1 μmol dpm$^{-1}$ in the Mertz polynya, whereas for large particles the averages were 35 ± 10 μmol dpm$^{-1}$ (two stations with ratios >130 μmol dpm$^{-1}$ not included) and 6 ± 2 μmol dpm$^{-1}$, for the Dalton and the Mertz polynya, respectively. At 300 m, the POC:$^{234}$Th ratio for both size classes and polynyas was on average ~12 μmol dpm$^{-1}$. Despite some variability, the shallow POC:$^{234}$Th ratios in small and large particles were comparable (within a factor of 2). To derive the POC fluxes using the $^{234}$Th deficits, we used the POC:$^{234}$Th ratios measured in the small particles in both polynyas. The rationale behind this is the fact that in

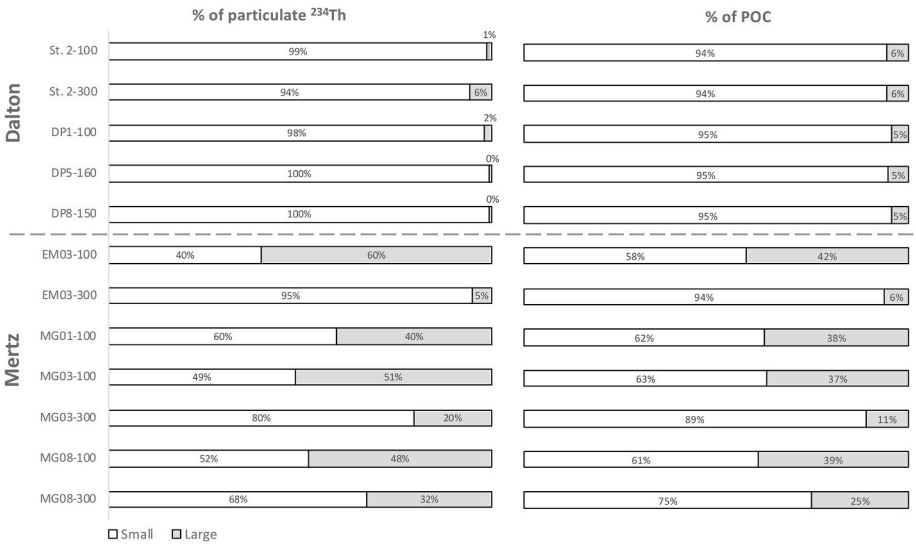


**Fig. 9.** Particulate thorium-234 ($^{234}$Th) and particulate organic carbon (POC) fractionation between small (1–53 μm) and large (>53 μm) particles at different stations and depths in the Dalton and Mertz polynyas. Note that the number next to the station name refers to the sampling depth (e.g., St.2-100 refers to samples collected at St.2 at 100 m depth).

the Dalton polynya $^{234}$Th activities in the large particles were very low (Fig. 9) leading to unreliable large POC:$^{234}$Th ratios (>130 μmol dpm$^{-1}$) compared to global open ocean POC:$^{234}$Th ratios (Puigcorbé et al., 2020) and in the Mertz polynya we did not find significant differences between the POC:$^{234}$Th ratios measured in small and large particles ($p = 0.053$).

### 3.7. Ammonium in seawater

The distribution of ammonium in seawater (Fig. 10) mimicked the POC profiles observed for the polynyas (Fig. 4). Ammonium concentration in the Mertz ($0.4 \pm 0.5$ μmol L$^{-1}$) and Ninnis polynyas ($0.5 \pm 0.6$ μmol L$^{-1}$) were not significantly different from each other ($p = 0.9$), but were significantly higher than in the Dalton polynya ($0.2 \pm 0.2$ μmol L$^{-1}$) and the off-shelf sites ($0.3 \pm 0.3$ μmol L$^{-1}$) ($p < 0.01$ for both). The Dalton and the off-shelf sites were not significantly different ($p = 0.2$).

## 4. Discussion

This study provides biogeochemical data from a climate sensitive and under sampled region around Antarctica. A limited number of POC sampling efforts have been conducted in East Antarctica, and $^{234}$Th quantification is extremely rare (Fig. 11). Since marine productivity in coastal East Antarctica is highly sensitive to changes in the icescape (Shadwick et al., 2014; Liniger et al., 2020), we need a robust baseline from which future changes can be evaluated. Below, we discuss the distribution and export of POC by looking into differences in primary production, the degradation state of organic matter and its nutritional value, as well as the role of heterotrophic communities across the different sampling locations.

### 4.1. Does primary production influence the vertical distribution and export of carbon?

Organic particles in the ocean originate from phytoplankton primary

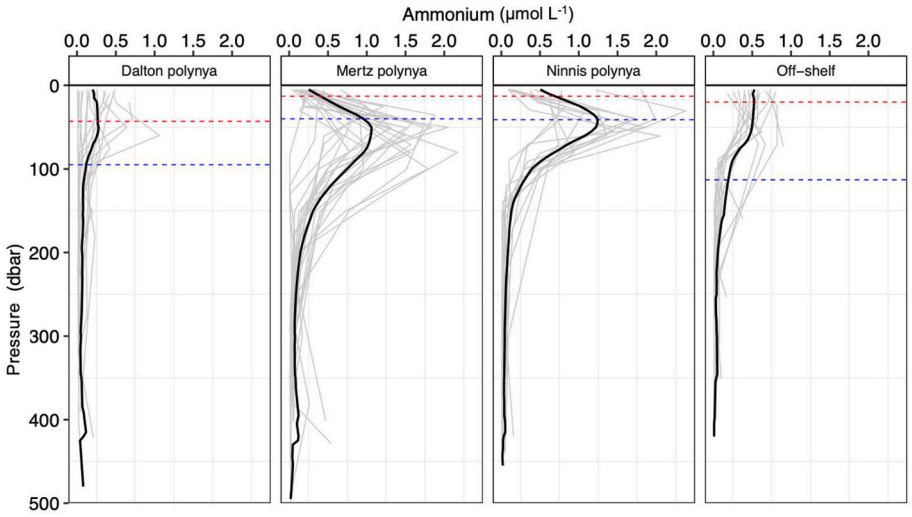


**Fig. 10.** Concentration of ammonium (μmol L$^{-1}$) in the Dalton, Mertz, and Ninnis polynyas, and at the off-shelf sites. Grey lines represent ammonia concentrations as measured from the CTD bottle samples. Solid black line indicates mean ammonium concentration across all stations and averaged every 5 dbar. Blue dashed horizontal line represents the average euphotic depth. Red dashed horizontal line represents the average mixed layer depth.

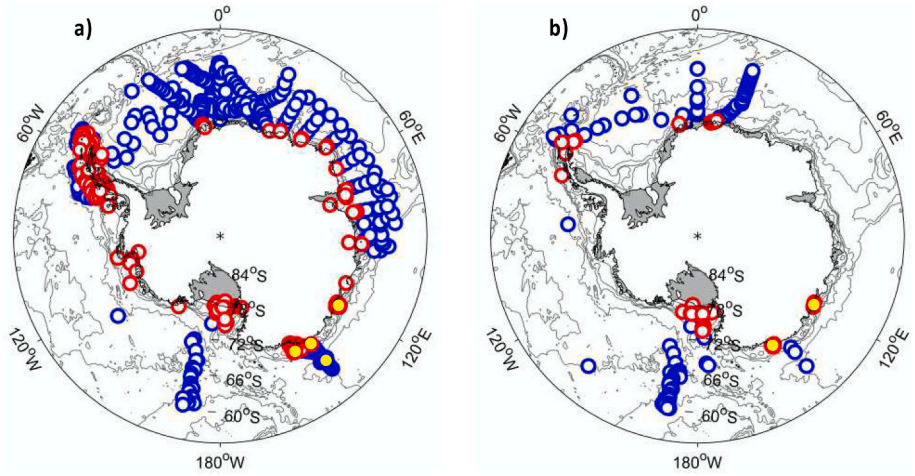


**Fig. 11.** Locations south of 60°S where POC a) and $^{234}$Th b) have been reported in the literature. Red circles indicate locations shallower than 1000 m, while blue circles indicate locations deeper than 1000 m. Circles with a yellow centre indicate locations included in this study. Data plotted in panel a) have been obtained from Evers-King et al. (2017) with additional data from Davis (2019), Mongin (2010), Pasquer et al., 2010, CLIVAR-SR3 (Tom Trull *pers. comm.),* Nodder and Waite (2003), Trull and Armand (2013), Romankevich and Peresypkin (1994), Nemirovskaya et al. (2013), Nemirovskaya and Chemyavskii (2011), Collier et al. (2000), Castro and González-Castro (2003), Brandt et al. (2011) and Alderkamp et al. (2012b). The locations plotted in panel b) have been extracted from Puigcorbé et al. (2020) with additional data from Charette and Buesseler (2000), Langone et al. (1997), Rutgers van der Loeff (2007) and Usbeck et al. (2002).

production. Moreau et al. (2019) recorded high and site-specific differences in Chl-a, phytoplankton biomass and NCP within the Mertz, Ninnis, and Dalton polynyas during the same voyage. Here we examine if the high primary production translates to substantial presence and export of POC along the water column. Within the polynyas, the highest average POC concentrations were measured in the Ninnis polynya followed by the Mertz and lastly the Dalton polynyas (Table 1, Fig. 4). In the Mertz and Ninnis polynyas, POC concentration increased with depth down to the deep Chl-a maximum depth (31 ± 9 m in the Mertz polynya and 33 ± 10 m in the Ninnis polynya; Moreau et al., 2019), and decreased thereafter (Fig. 4). In the Dalton polynya, three stations in the southeast of the polynya had much higher POC concentrations compared to the other stations sampled within the same polynya. These three stations with elevated POC in the Dalton polynya correspond to sites with higher Chl-a (Moreau et al., 2019).

Integrated Chl-a (top 200 m) was higher in the Mertz and Ninnis polynyas (158–507 mg Chl-a $m^{-2}$ and 152–453 mg Chl-a $m^{-2}$, respectively) compared to the Dalton polynya (9–304 mg Chl-a $m^{-2}$). Similarly, NCP was significantly higher in the Mertz and Ninnis polynyas (31–107 g C $m^{-2}$ and 36–69 g C $m^{-2}$, respectively) compared to the Dalton polynya (4–57 g C $m^{-2}$, Moreau et al., 2019). Integrated POC were roughly double in the Mertz and Ninnis polynyas compared to the Dalton polynya (Table 1). $^{234}$Th-derived POC export was only measured in the Mertz and Dalton polynyas, and there were significant differences between both polynyas: $^{234}$Th fluxes were 5-fold higher in the Mertz compared to the Dalton polynya, leading to POC export flux in the Mertz that was, on average, 5 times higher than in the Dalton polynya (16 ± 6 vs 3 ± 2 mmol C $m^{-2}$ $d^{-1}$, respectively, Table 2). By comparing the POC export fluxes to NPP we can estimate the efficiency of the export in both polynyas. NPP estimates were inferred from nitrate drawdown in the surface layer compared to the deeper winter layer (Moreau et al., 2019), which is suggested to be a valid approach in such high latitude areas (Moreau et al., 2013, Frasson et al., 2004). The opening of the polynyas started in September/October; however, the beginning of the productive season was considered to be mid/late-November based on inspection of satellite-derived ocean color and previous studies in the Dalton and Mertz polynyas (Arrigo et al., 2015; Liniger et al., 2020). Based on this assumption, we estimate that the export efficiency in the Mertz polynya was, on average, 15%, compared to 5% in the Dalton polynya.

The off-shelf sites were not examined in Moreau et al. (2019). However, the same fluorometer was used throughout the voyage, allowing us to extrapolate the relationship presented in Moreau et al. (2019) between seawater fluorescence and Chl-a to the off-shelf sites to determine if integrated POC distribution and integrated Chl-a were different between the polynyas and the off-shelf sites. Integrated Chl-a (top 200 m) at the off-shelf sites (62–96 mg Chl-a $m^{-2}$) were lower compared to the polynyas. Yet, at the off-shelf sites it was higher than those found during the CLIVAR-SR3 cruise in 2001 (35–37 mg Chl-a $m^{-2}$ at 64.9°S and 60.8°S, and 140°E, Kopczyńska et al., 2007), which followed the same transect at a similar time of the year (Nov–Dec). However, despite the higher values obtained in this study compared to the CLIVAR-SR3 cruise and the expected inter-annual variability, Chl-a and POC concentrations in the off-shelf region was markedly lower compared to the polynyas. Taken all together, we find that the high primary production observed in the Ninnis and Mertz polynyas (Moreau et al., 2019), led to higher vertical concentration and export of POC compared to the Dalton polynya and off-shelf sites.

### 4.2. POC:Chl-a ratio as a proxy of detrital or degraded organic matter relative to living phytoplankton

The POC:Chl-a ratio can be used to describe the relative proportion of organic material (living and non-living) relative to autotrophic organisms, where POC:Chl-a <100 mg $mg^{-1}$ indicates living phytoplankton, POC:Chl-a <200 mg $mg^{-1}$ indicates phytoplankton dominated particulate organic matter, and POC:Chl-a >200 mg $mg^{-1}$ is considered characteristic of detrital or degraded organic matter (Liénart et al., 2016; Thomalla et al., 2017; Arrigo et al., 2003). However, it is important to note that there can be high spatio-temporal variability in the POC:Chl-a ratios due to physiological photoacclimation, variations in the community composition and phytoplankton biomass (Behrenfeld et al., 2002, 2005, 2015).

At the off-shelf sites, degraded material (POC:Chl-a >200 mg $mg^{-1}$) was found below 100 m, shallower that what was observed in the polynyas. In the upper 200 m of the Mertz polynya, the POC:Chl-a ratio remained relatively constant (<100 mg $mg^{-1}$) suggesting the presence of living phytoplankton. Based on nutrient drawdown ratios and microscope analyses of the phytoplankton communities, diatoms (*Fragilariopsis curta* and *F. cylindrus*) dominated phytoplankton biomass in the Mertz polynya (Moreau et al., 2019), and these typically ice-associated diatoms could aggregate and be exported to deeper waters (Michels et al., 2008). Blooms of sea-ice and planktonic diatoms are often associated with enhanced POC export (Romero and Armand 2010; Roca-Martí et al., 2017; Leblanc et al., 2018). The high $^{234}$Th fluxes measured in the Mertz polynya (Fig. 8 and Table 2), where large particles contributed to a larger extent to particulate $^{234}$Th and POC compared to the Dalton (Fig. 9), are in line with the dominance of diatoms and the stronger influence of ice melt in that polynya (Moreau et al., 2019). Transfer efficiencies between 100 and 300 m (i.e., POC flux at 300 m/POC flux at 100 m) could only be calculated at three stations in the Mertz polynyas but they were, in all cases, >75%, indicating that a large proportion of the POC leaving the productive layer reached depths of

300 m. Such high transfer efficiencies have been reported in highly productive areas of the North Atlantic and the Southern Ocean (e.g., Buesseler and Boyd, 2009) usually related to diatom blooms. Healthy diatoms have been found well below the euphotic zone (e.g. down to 4, 000 m in Agusti et al., 2015) which, together with POC:Chl-a ratios $<$100 mg mg$^{-1}$, suggest that living diatoms may have contributed to carbon export in the Mertz polynya. Diatoms have a high silica content (Brzezinski 1985), and their blooms can lead to strong silicic acid drawdown, as was observed in the Mertz polynya (Moreau et al., 2019). Also, diatoms often produce biological glues, which may promote aggregation and hence faster sinking rates and lower attenuation with depth (Passow et al., 1994; Smetacek et al., 2012), with studies reporting diatom sinking rates that can exceed 700 m d$^{-1}$ (Asper and Smith 2003; Agusti et al., 2015).

The POC:Chl-a ratios in the Dalton and Ninnis polynyas gradually increased with depth and degraded material (POC:Chl-a $>$ 200 mg mg$^{-1}$) was measured at depths greater than 150 m (Fig. 6). A mixed phytoplankton community of diatoms and small flagellates including *Phaeocystis antarctica* dominated in the Ninnis polynya, whilst small flagellates including *P. antarctica* dominated in the Dalton polynya (Moreau et al., 2019). In the Dalton polynya we observed that the quasi-totality (94–100%) of the particulate $^{234}$Th and POC was found in the small particles (Fig. 9), which agrees with dominance of smaller phytoplankton. The higher POC:Chl-a ratio in the Ninnis and Dalton polynyas coupled with the presence of a mixed phytoplankton community compared to the Mertz polynya suggest that the Ninnis and Dalton polynyas may have been at a more advanced stage of bloom at the time of sampling. Whilst DiTullio et al. (2000) demonstrated that in the Ross Sea *P. antarctica* blooms are exported rapidly during the early spring bloom, we find that the Dalton polynya had lower POC concentrations and POC export compared to the Mertz polynya and lower POC concentrations compared to the Ninnis polynya, where diatoms would have been the drivers of the enhanced POC concentrations. Our results agree with those of Kim et al. (2015), who found that, even in the ice-covered areas surrounding the Amundsen Sea polynya where diatoms dominated the plankton community, the POC flux was larger than inside the actual polynya, where *P. antarctica* was dominant.

### 4.3. C:N ratio as a proxy for the nutritional quality of organic matter

The C:N ratio in the natural environment is plastic and, under nutrient replete conditions, values of C:N can diverge from the canonical 6.6 Redfield ratio, ranging from 3 to 17 due to species-specific responses, differences in growth conditions or analytical techniques (Geider and La Roche 2002; Arrigo 2005; Garcia et al., 2018). Yet, a low C:N ratio is generally attributed to N enrichment and the presence of 'fresher' material, whereas a higher C:N ratio is considered to indicate preferential remineralization of N and a more degraded pool. The C:N ratios measured here were within the reported range of phytoplankton growing under nutrient-replete conditions (Geider and La Roche 2002; Arrigo 2005; Garcia et al., 2018), but they did differ between sites. The C:N ratio in the Ninnis polynya (5.7 $\pm$ 0.7) was the closest one to the Redfield ratio (6.6), while ratios below the Redfield ratio were observed at the other sites (Mertz polynya 4.8 $\pm$ 0.9, Dalton polynya 4.8 $\pm$ 1.2, and off-shelf sites 4.0 $\pm$ 0.6; Fig. 7). The C:N ratios measured in all three polynyas fall within the natural variability observed in the euphotic layer of the Ross Sea (5.4–9.2; Fabiano et al., 1993) and the Amundsen Sea polynya (6.3–9.2; Kim et al., 2018), whereas the off-shelf sites are slightly below those ranges. The stoichiometry of remineralization is a function of the nutritional demand of the heterotrophic population (Turley and Mackie 1994; Sterner and Elser 2002; Burkhardt et al., 2014; Letscher and Moore 2015). In some areas of the Southern Ocean, heterotrophic bacteria have been shown to be carbon limited (Church et al., 2000; Obernosterer et al., 2015). Therefore, it is possible that heterotrophic bacteria were preferentially consuming carbon at the off-shelf sites, leading to lower C:N ratios, which could also be the cause of the decreasing C:N ratios with depth in the Dalton polynya.

### 4.4. Ammonium as an indicator of heterotrophic communities

The high concentration of ammonium (Fig. 10) could indicate the presence of heterotrophic communities. The production of ammonium by bacteria and zooplankton is an important process in the marine nitrogen cycle as phytoplankton (both eukaryotes and cyanobacteria) utilize ammonium before nitrate due to the reduced energy costs. However, heterotrophic bacteria are also competitors with phytoplankton for ammonium (Hoch and Kirchman 1995). The concentration of ammonium measured in the present study fall within the summer values measured previously in the Southern Ocean (~0.05–1.03 μmol L$^{-1}$, Bianchi et al., 1997; Mengesha et al., 1998), around the Antarctic Peninsula (0.9–10 μmol L$^{-1}$, Koike et al., 1986; Owens et al., 1991; Karl et al., 1996; Garibotti et al., 2003), and in the Ross Sea (4 μmol L$^{-1}$, Gordon et al., 2000). The highest ammonium concentrations were found in the Ninnis and the Mertz polynyas (2.2–2.4 μmol L$^{-1}$) in line with the deep Chl-a and POC maxima. As expected, the lower POC in the Dalton polynya and the off-shelf sites were accompanied by lower ammonium concentrations (0.9–1.1 μmol L$^{-1}$).

As ammonium is released by both the bacterial and zooplankton communities, it is not possible to distinguish the influence of these heterotrophic communities on the distribution of POC. However, the distribution of ammonium resembles that of POC, which indicates that grazing and/or remineralization track POC, rather than being concentrated at a particular depth horizon or light level. Moreau et al. (2020) recently showed that grazers consume about 90% of the phytoplankton in the sea-ice zone of the Southern Ocean. The fact that the ammonium profiles mirrored the vertical distribution of POC could suggest that POC may not escape the heterotrophic community very effectively while sinking, which may lead to low carbon export efficiency. In the Dalton polynya the average export efficiency was 5%, similar to those observed in oligotrophic areas (e.g., Puigcorbé et al., 2017b). The decreasing C:N ratios with depth suggest preferential remineralization of C by bacteria (e.g., Church et al., 2000). However, export efficiency in the Mertz polynya was 15%, where we also estimated high transfer efficiencies down to 300 m. We note two possible scenarios: 1) lower POC in the Dalton polynya attracts lesser heterotrophic communities compared to Mertz polynya, leading to lower ammonium concentration and lower export efficiency in the Dalton, and 2) the differences in planktonic community composition between the Dalton polynya, which was dominated by small flagellates, and the Mertz polynya, which was dominated by diatoms, may drive differences in export efficiency.

## 5. Conclusion and future work

The higher primary production within the Mertz, Ninnis and Dalton polynyas resulted in higher vertical concentrations and stocks of POC along the water column within the polynyas compared to the off-shelf sites. As shown in other studies, primary production can vary greatly between polynyas. Here, vertical concentration of POC was greater in the Mertz and Ninnis polynyas compared to the Dalton polynya, and this translated to ~5 times higher carbon export in the Mertz compared to the Dalton on average. The POC:Chl-a ratios of $<$200 mg mg$^{-1}$ in the upper 150 m in the Mertz, Ninnis and Dalton polynyas suggests that organic particles consisted largely of phytoplankton. However, the concentrations and stocks of POC were found to be significantly different amongst the polynyas, suggesting that the factors controlling the distribution of POC would differ between them, thereby influencing carbon export. In the Mertz polynya, a relatively constant low POC:Chl-a ratio down to 200 m indicates that POC largely consisted of fresh material, which together with the high transfer efficiency observed in that polynya and information on the algae community, suggests that living diatoms contributed to carbon export that largely persisted throughout the upper mesopelagic zone. In contrast, in the Ninnis, Dalton and off-

shelf sites, the POC:Chl-a ratios increased with depth pointing towards an increase in degraded material. The C:N ratios measured in this study suggest a high nutritional quality of the organic matter, which would encourage the presence of heterotrophic communities. Interestingly, the ammonium profiles follow the POC profiles, suggesting that these heterotrophic communities were degrading the POC throughout the water column.

The polynya-specific differences highlighted here provide an interesting framework for future work. It has been shown that, under future climate scenarios with increased global ocean temperatures, smaller phytoplankton communities could be favored (Montes-Hugo et al., 2009; Morán et al., 2010). If phytoplankton community structure in the Mertz were to switch towards smaller sized cells akin to the Dalton polynya, then our study suggests that the biologically mediated carbon export in these coastal polynyas may decrease. However, patterns of remineralization and grazing may also change depending on the response of the bacterial and zooplankton communities to temperature and resource supply (e.g., iron and dissolved organic carbon availability to phytoplankton, and metabolic demand of zooplankton and bacteria), both of which are highly uncertain. Therefore, quantifying the micronutrients and dissolved organic carbon content in this region, coupled with the rate of bacterial remineralization of sinking particles and zooplankton community dynamics will provide better insight into carbon cycling and improve its predictability in these highly productive regions under future climate scenarios.

## Declaration of competing interest

The authors declare that they have no known competing financial interests or personal relationships that could have appeared to influence the work reported in this paper.

## Data availability

Data presented in this study can be sourced from https://metadata.imas.utas.edu.au/geonetwork/srv/eng/metadata.show?uuid=02364e10-ebc0-463a-b690-2c4ed643733c.

## Acknowledgments

This study was supported by the Australian Government's Cooperative Research Centres through the Antarctic Climate and Ecosystem Cooperative Research Centre, the Australian Antarctic Division research projects AAS 4131 and 4291, and the Institute for Marine and Antarctic Studies, University of Tasmania. L. Ratnarajah also received support from BYONIC (ERC award number 724289). D. Lannuzel was supported by an Australian Research Council Future Fellowship (Project ID L0026677). S. Moreau and C. Genovese were supported by the Australian Research Council's Special Research Initiative for Antarctic Gateway Partnership (Project ID SR140300001). V. Puigcorbé was supported by Edith Cowan University through an Early Career Researcher Grant (G1003456) and an ECU-Collaboration Enhancement Scheme grant (G1003362). V. Puigcorbé received the support of a fellowship from "la Caixa" Foundation (ID 100010434) and from the European Union's Horizon 2020 research and innovation programme under the Marie Skłodowska-Curie grant agreement No 847648 (fellowship code 105183). M. Roca-Martí was supported by funding from the Woods Hole Oceanographic Institution's Ocean Twilight Zone study and the Ocean Frontier Institute. Thanks to Thomas Rodemann at the Central Science Laboratory, University of Tasmania, Australia for the POC analyses, to Stephen Tibben and the Marine National Facility, CSIRO, Australia for ammonium analyses, to Walter Geibert, Alfred Wegener Institute (Germany), for thorium recovery analyses, and to Tom Trull for providing critical comments on the development of this manuscript. We acknowledge the use of imagery from the NASA Worldview application (https://worldview.earthdata.nasa.gov), part of the NASA Earth Observing System Data and Information System (EOSDIS). The IAEA is grateful for the support provided to its Environment Laboratories by the Government of the Principality of Monaco. This work acknowledges the 'Severo Ochoa Centre of Excellence' accreditation (CEX2019-000928-S). Lastly, the authors would like to thank the officers and crew of the RSV Aurora Australis for their logistical support.

## Appendix A. Supplementary data

Supplementary data to this article can be found online at https://doi.org/10.1016/j.dsr.2022.103899.

## References

Agusti, S., González-Gordillo, J.I., Vaqué, D., Estrada, M., Cerezo, M.I., Salazar, G., Gasol, J.M., Duarte, C.M., 2015. Ubiquitous healthy diatoms in the deep sea confirm deep carbon injection by the biological pump. Nat. Commun. 6, 1–8.

Alderkamp, A., Mills, M., van Dijken, G.L., Laan, P., Thuróczy, C.E., Gerringa, L.J.A., De Baar, H.J.W., Payne, C.D., Visser, R.J.W., Buma, A.G.J., Arrigo, K.R., 2012a. Iron from melting glaciers fuels phytoplankton blooms in the Amundsen Sea (Southern Ocean): phytoplankton characteristics and productivity. Deep Sea Res. Part II Top. Stud. Oceanogr. 71–76 (15), 32–48.

Alderkamp, A., Mills, M., van Dijken, G.L., Laan, P., Thuróczy, C.E., Gerringa, L.J.A., De Baar, H.J.W., Payne, C.D., Visser, R.J.W., Buma, A.G.J., Arrigo, K.R., 2012b. Surface water properties, phytoplankton composition and photosynthesis rates of Amundsen Sea sites. PANGAEA. https://doi.org/10.1594/PANGAEA.806489.

Andersen, P.S., 1993. Evidence for an Antarctic winter coastal polynya. Antarct. Sci. 5 (2), 221–226.

Arrigo, K.R., 2005. Marine microorganisms and global nutrient cycles. Nature 437, 349–355.

Arrigo, K.R., van Dijken, G.L., 2003. Phytoplankton dynamics within 37 Antarctic coastal polynya systems. J. Geophys. Res. 108 (C8), 3271 27-22 27-18.

Arrigo, K.R., Robinson, D.H., Dunbar, R.B., Leventer, A.R., Lizotte, M.P., 2003. Physical control of chlorophyll a, POC, and TPN distributions in the pack ice of the Ross Sea, Antarctica. J. Geophys. Res.: Oceans 108 (C10).

Arrigo, K.R., van Dijken, G.L., Strong, A.L., 2015. Environmental controls of marine primary productivity hot spots around Antarctica. J. Geophys. Res.: Oceans 120, 5545–5565.

Asper, V.L., Smith, W.O., 2003. Abundance, distribution and sinking rates of aggregates in the Ross Sea, Antarctica. Deep-Sea Res. I: Oceanogr. Res. Pap. 50 (1), 131–150.

Behrenfeld, M.J., Boss, E.S., 2006. Beam attenuation and chlorophyll concentration as alternative optical indices of phytoplankton biomass. J. Mar. Res. 64, 431–451.

Behrenfeld, M.J., Marañón, E., Siegel, D.A., Hooker, S.B., 2002. Photoacclimation and nutrient-based model of light-saturated photosynthesis for quantifying oceanic primary production. Mar. Ecol. Prog. Ser. 228, 103–117.

Behrenfeld, M.J., Boss, E., Siegel, D.A., Shea, D.M., 2005. Carbon-based ocean productivity and phytoplankton physiology from space. Glob. Biogeochem. 19.

Behrenfeld, M.J., O'Malley, R.T., Boss, E.S., Westberry, T.K., Graff, J.R., Halsey, K.H., et al., 2015. Revaluating ocean warming impacts on global phytoplankton. Nat. Clim. Change 6, 323–330.

Behrenfeld, M.J., Gaube, P., Della Penna, A., O'Malley, R.T., Burt, W.J., Yongxiang, H., Bontempi, P.S., Steinberg, D.K., Boss, E.S., Siegel, D.A., Hostetler, C.A., Tortell, P.D., Doney, S.C., 2019. Global satellite-observed daily vertical migrations of ocean animals. Nature 576, 257–261.

Benitez-Nelson, C.R., Buesseler, K.O., Rutgers van der Loeff, M., Andrews, J., Ball, L., Crossin, G., Charette, M.A., 2001. Testing a new small-volume technique for determining $^{234}$Th in seawater. J. Radioanal. Nucl. Chem. 248, 795–799.

Bianchi, M., Feliatra, F., Tréguer, P., Vincendeau, M., Morvan, J., 1997. Nitrification rates, ammonium and nitrate distribution in the upper layers of the water column and in sediments of the Indian sector of the Southern Ocean. Deep Sea Res, II: Topic. Stud. Oceanogr. 5, 1017–1032.

Bishop, J.K.B., 1999. Transmissometer measurement of POC. Deep Sea Res. I: Oceanogr. Res. Pap. 46, 353–369.

Boyd, P.W., Ellwood, M.J., Tagliabue, A., Twining, B.S., 2017. Biotic and abiotic retention, recycling and remineralization of metals in the ocean. Nat. Geosci. 10, 167–173.

Brandt, A., Bathmann, U., Brix, S., Cisewski, B., Flores, H., Göcke, C., Janussen, D., Krägefsky, S., Kruse, S., Leach, H., Linse, k., Pakhomov, E.A., Peeken, I., Riehl, T., Sauter, E.-J., Sachs, O., Schüller, M., Schröld, M., Schwabe, E., Strass, V.H., van Franeker, J.A., Wilmsen, M., 2011. (Table 1) Particulate Organic Nitrogen and Carbon Concentration, Seston Abundance and Chlorophyll a Content at Station PS71/039 on Maud Rise. PANGAEA. https://doi.org/10.1594/PANGAEA.847268.

Briggs, N., Perry, M.J., Cetinić, I., Lee, C., D'Asaro, E., Gray, A.M., et al., 2011. High-resolution observations of aggregate flux during a sub-polar North Atlantic spring bloom. Deep-Sea Res., Part A *I*58, 1031–1039.

Brzezinski, M.A., 1985. The Si:C:N ratio of marine diatoms: interspecific variability and the effect of some environment variables. J. Phycol. 21, 347–357.

Buesseler, K.O., Boyd, P.W., 2009. Shedding light on processes that control particle export and flux attenuation in the twilight zone of the open ocean. Limnol. Oceanogr. 54 (4), 1210–1232.

Burkhardt, B.G., Watkins-Brandt, K.S., Defforey, D., Payton, A., White, A.E., 2014. Remineralization of phytoplankton-derived organic matter by natural populations of heterotrophic bacteria. Mar. Chem. 163, 1–9.
Castro, C.G., González-Castro, C., 2003. Nutrients Measured on Water Bottle Samples at Station Fruela96_195.2. PANGAEA. https://doi.org/10.1594/PANGAEA.101380.
Cetinić, I., Perry, M.J., Briggs, N.T., Kallin, E., D'Asaro, E.A., Lee, C.M., 2012. Particulate organic carbon and inherent optical properties during 2008 North Atlantic Bloom Experiment. J. Geophys. Res.: Oceans 117, C06028.
Charette, M.A., Buesseler, K.O., 2000. Does iron fertilization lead to rapid carbon export in the Southern Ocean? G-cubed 1, 1041.
Church, M.J., Hutchins, D.A., Ducklow, H.W., 2000. Limitation of bacterial growth by dissolved organic matter and iron in the Southern Ocean. Appl. Environ. Microbiol. 66 (2), 455–466.
Clevenger, S.J., R Benitez-Nelson, C., Drysdale, J., Pike, S., Puigcorbé, V., Buesseler, K.O., 2021. Review of the analysis of $^{234}$Th in small volume (2-4 L) seawater samples: improvements and recommendations. J. Radioanal. Nucl. Chem. 329, 1–13.
Collier, R.W., Dymond, J.R., Honjo, S., Manganini, S.J., François, R., Dunbar, R.G., 2000. Particle Fluxes of NBP96-4A_MS6_trap. PANGAEA. https://doi.org/10.1594/PANGAEA.92818.
Dall'Olmo, G., Dingle, J., Polimene, L., Brewin, R.J.W., Claustre, H., 2016. Substantial energy input to the mesopelagic ecosystem from the seasonal mixed-layer pump. Nat. Geosci. 9, 820–823.
Davis, D.M., 2019. Particulate organic matter elemental analysis, mixed layer, during the K-Azis voyage of the Aurora Australis au1603. Australian Antarctic Data Centre. https://doi.org/10.26179/5cf49be15fc98 dataset.
de Boyer Montégut, C., Madec, G., Fischer, A.S., Lazar, A., Iudicone, D., 2004. Mixed layer depth over the global ocean: an ecxamination of profile data and a profile-based climatology. J. Geophys. Res. 109, 1–20.
Deppeler, S., Davidson, A., 2017. Southern Ocean phytoplankton in a changing climate. Front. Mar. Sci. 4 (40), 1–29.
DiTullio, G.R., Grebmeier, J.M., Arrigo, K.R., Lizotte, M.P., Robinson, D.H., Leventer, A., Barry, J.P., VanWoert, M.L., Dunbar, R.B., 2000. Rapid and early export of Phaeocystis Antarctica bloom in the Ross Sea, Antarctica. Nature 404, 595–598.
Ducklow, H.W., Wilson, S.E., Post, A.F., Stammerjohn, S.E., Erickson, M., Lee, S.H., Lowry, K.E., Sherrel, R.M., Yager, P.L., 2015. Particle flux on the continental shelf in the Amundsen Sea polynya and western antarctic Peninsula. Elementa: Sci. Anthropocene 1–20.
Evers-King, H., Martinez-Vicente, V., Brewin, R.J.W., Dall'Olmo, G., Hickman, A.E., Jackson, T., Kostadinove, T.S., Krasemann, H., Loisel, H., Röttgers, R., Roy, S., Stramski, D., Thomalla, S., Platt, T., Sathyendranath, S., 2017. Front. Mar. Sci. 4, 251.
Fabiano, M., Povero, P., Danovaro, R., 1993. Distribution and composition of particulate organic matter in the Ross Sea (Antarctica). Polar Biol. 13, 525–533.
Falkowski, P.G., Barber, R.T., Smetacek, V., 1998. Biogeochemical controls and feedbacks on ocean primary production. Science 281 (5374), 200–206.
Fan, G., Han, Z., Ma, W., Chen, S., Chai, F., Mazloff, M.R., Pan, J., Zhang, H., 2020. Southern Ocean carbon export efficiency in relation to temperature and primary productivity. Sci. Rep. 10 (13494), 1–11.
Fraser, A.D., Massom, R.A., Michael, K.J., Galton-Fenzi, B., Lieser, J.L., 2012. East Antarctic landfast sea ice distribution and variability, 2000-08. Am. Meteorol. Soc. 25 (4), 1137–1156.
Frasson, A., Chierici, M., Anderson, L.G., David, R., 2004. Transformation of carbon and oxygen in the surface layer of the eastern Atlantic sector of the Southern Ocean. Deep-Sea Res. II 51, 2757–2772.
Garcia, N.S., Sexton, J., Riggins, T., Brown, J., Lomas, M.W., Martiny, A.C., 2018. High variability in cellular stoichiometry of carbon, nitrogen and phosphorus within classes of marine eukaryotic phytoplankton under sufficient nutrient conditions. Front. Microbiol. 9 (543), 1–10.
Gardner, W.D., Chung, S.P., Richarson, M.J., Walsh, I.D., 1995. The oceanic mixed layer pump. Deep Sea Res. Part II Top. Stud. Oceanogr. 42, 757–775.
Gardner, W.D., Richarson, M.J., Mishonov, A.V., Biscaye, P.E., 2018a. Global comparison of benthic nepheloid layers based on 52 years of T nephelometer and transmissometer measurements. Prog. Oceanogr. 168, 100–111.
Gardner, W.D., Richarson, M.J., Mishonov, A.V., 2018b. Global assessment of benthic nepheloid layers and linkage with upper ocean dynamics. Earth Planet Sci. Lett. 482, 126–134.
Garibotti, I.A., Vernet, M., Ferrario, M.E., Smith, R.C., Ross, R.M., Quentin, L.B., 2003. Phytoplankton spatial distribution patterns along the western antarctic Peninsula (Southern Ocean). Mar. Ecol. Prog. Ser. 261, 21–39.
Geider, R.J., La Roche, J., 2002. Redfield revisited: variability of C:N:P in marine microalgae and its biochemical basis. Eur. J. Phycol. 37, 1–17.
Gerringa, L.J.A., Alderkamp, A.-C., Laan, P., Thuróczy, C.E., De Baar, H.J.W., Mills, M. M., van Dijken, G.L., van Haren, H., Arrigo, K.R., 2012. Iron from melting glaciers fuels the phytoplankton blooms in Amundsen Sea (Southern Ocean): iron biogeochemistry. Deep Sea Res, II: Topic. Stud. Oceanogr. 71–76 (15), 16–31.
Giles, A.B., 2017. The Mertz Glacier Tongue, East Antarctica. Changes in the past 100 years and its cyclic nature - past, present and future. Rem. Sens. Environ. 191, 30–37.
Gordon, L.I., Codispoti, L.A., Jennings Jr., J.C., Millero, F.J., Morrison, J.M., Sweeney, C., 2000. Seasonal evolution of hydrographic properties in the Ross Sea, Antarctica, 1996–1997. Deep Sea Res, II: Topic. Stud. Oceanogr. 47, 3095–3117.
Henson, S., Sander, R., Madsen, E., 2012. Global patterns in efficiency of particulate organic carbon export and transfer to the deep ocean. Global. Biogeochem. Cycles 26 (1). https://doi.org/10.1029/2011GB004099.
Henson, S.A., Yool, A., Sanders, R., 2015. Variability in efficiency of particulate organic carbon export: a model study. Global Biogeochem. Cycles 29 (1), 33–45.
Henson, S., Le Moigne, F., Giering, S., 2019. Drivers of carbon export efficiency in the global ocean. Global Biogeochem. Cycles 33, 891–903.
Herraiz-Borreguero, L., Lannuzel, D., van der Merwe, P., Treverrow, A., Pedro, J.B., 2016. Large flux of iron from the amery ice shelf marine ice to pyrdz Bay, East Antarctica. J. Geophys. Res.: Oceans 121 (8), 6009–6020.
Hoch, M.P., Kirchman, D.L., 1995. Ammonium uptake by heterotrophic bacteria in the Delaware estuary and adjacent coastal waters. Limnol. Oceanogr. 40 (5), 886–897.
Hoppema, M., Anderson, L.G., 2007. Biogeochemistry of Polynyas and Their Role in Sequestration of Anthropogenic Constituents. Polynyas: Windows to the World, 74. Elsevier, pp. 193–221. https://www.sciencedirect.com/science/article/pii/S0422989406740065, 2007.
Karl, D.M., Christian, J.R., Dore, J.E., Letelier, R.M., 1996. Microbiological Oceanography in the Region West of the Antarctic Peninsula: Microbial Dynamics, Nitrogen Cycle and Carbon Flux. American Geophysical Union, Washington, DC.
Karnovsky, N., Ainley, D.G., Lee, P., 2007. Chapter 12 the Impact and Importance of Production in Polynyas to Top-Trophic Predators: Three Case Histories, vol. 74. Elsevier Oceanography Series, pp. 391–410.
Kérouel, R., Aminot, A., 1997. Fluorometric determination of ammonia in sea and estuaring waters by direct segmented flow analysis. Mar. Chem. 57, 265–275.
Kim, M., Hwang, J., Kim, H.J., Kim, D., Yang, E.J., Ducklow, H.W., Hyoung, S.L., Lee, S. H., Park, J., Lee, S.H., 2015. Sinking particle flux in the sea icea zone of the Amundsen Shelf, Antarctica. Deep Sea Res. Oceanogr. Res. Pap. 101, 110–117.
Kim, B., Lee, S.H., Ha, S.Y., Jung, J., Kim, T., Yang, E.J., Jo, N., Lim, Y., Park, J., Lee, S. H., 2018. Vertical distribution of macromolecular composition of particulate organic matter in the water column of the Amundsen Sea Polynya during the summer of 2014. J. Geophys. Res.: Oceans 123, 1393–1405.
Knap, A., Michaels, A., Close, A., 1994. JGOFS Protocols, vol. 198. JGOFS Plan. Off. Woods Hole, MA, US.
Koike, I., Holm-Hansen, O., Biggs, D.C., 1986. Inorganic nitrogen metabolism by Antarctic phytoplankton with special reference to ammonium cycling. Mar. Ecol. Prog. Ser. 30, 105–116.
Kopczyńska, E.E., Savoye, N., Dehairs, F., Cardinal, D., Elskens, M., 2007. Spring phytoplankton assemblages in the Southern Ocean between Australia and Antarctica. Polar Biol. 31 (1), 77–78.
Langone, L., Frignani, M., Cochran, J.K., Ravaioli, M., 1997. Scavenging processes and export fluxes close to a retreating seasonal ice margin (Ross Sea, Antarctica). Water Air Soil Pollut. 99, 705–715.
Lannuzel, D., Bowie, A.R., van der Merwe, P.C., Townsend, A.T., Schoemann, V., 2011. Distribution of dissolved and particulate metals in Antarctic sea ice. Mar. Chem. 124 (1–4), 134–146.
Laws, E.A., Maiti, K., 2019. The relationship between primary production and export production in the ocean: effects of time lags and temporal variability. Deep Sea Res. I: Oceanogr. Res. Pap. 148, 100–107.
Le Moigne, F.A.C., Henson, S., Cavan, E., Georges, C., Pabortsava, K., Achterberg, E.P., Ceballos-Romero, E., Zubkov, M.V., Sanders, R.J., 2016. What causes the inverse relationship between primary production and export efficiency in the Southern Ocean. Geophys. Res. Lett. 43, 4457–4466.
Leblanc, K., Quéguiner, B., Diaz, F., Cornet, V., Michel-Rodriguez, M., de Madron, X.D., Bowler, C., Malviya, S., Thyssen, M., Grégori, G., Rembauville, M., Grosso, O., Poulain, J., de Vargas, C., Pujo-Pay, M., Conan, P., 2018. Nanoplanktonic diatoms are globally overlooked but play a role in spring blooms and carbon export. Nat. Commun. 9 (953), 1–12.
Lee, S.H., Hwang, J., Ducklow, H.W., Hahm, D., Lee, S.H., Kim, D., Hyun, J.H., Park, J., Ha, H.K., Kim, T.W., Yang, E.J., Shin, H.C., 2017. Evidence of minimal carbon sequestration in the productive Amundsen Sea polynya. Geophys. Res. Lett. 44, 7892–7899.
Letscher, R.T., Moore, J.K., 2015. Preferential remineralization of dissolved organic phosphorus and non-Redfield DOM dynamics in the global ocean: impacts on marine productivity, nitrogen fixation and carbon export. Global Biogeochem. Cycles 29, 325–340.
Liénart, C., Susperregui, N., Rouaud, V., Cavalheiro, J., David, V., Del Amo, Y., Duran, R., Lauga, B., Monperrus, M., Pigot, T., Bichon, S., Charlier, K., Savoye, N., 2016. Dynamics of particulate organic matter in a coastal system characterized by the occurrence of marine mucilage – a stable isotope study. J. Sea Res. 116, 12–22.
Lin, H., Rauschenberg, S., Hexel, C.R., Shaw, T.J., Twining, B.S., 2011. Free-drifting icebergs as sources of iron to the Weddell Sea. Deep Sea Res. Part II Top. Stud. Oceanogr. 58 (11–12), 1392–1406.
Liniger, G., Strutton, P.G., Lannuzel, D., Moreau, S., 2020. Calving event led to changes in phytoplankton bloom phenology in the Mertz Polynya, Antarctica. J. Geophys. Res.: Oceans 125, e2020JC016387.
Maiti, K., Charette, M., Buesseler, K.O., Kahru, M., 2013. An inverse relationship between production and export efficiency in the Southern Ocean. Geophys. Res. Lett. 40, 1557–1561.
Marinov, I., Gnanadesikan, A., Toggweiler, J.R., Sarmiento, J.L., 2006. The Southern Ocean biogeochemical divide. Nature 441 (7096), 964–967.
Martin, J., 1990. Glacial-interglacial $CO_2$ change: the iron hypothesis. Paleoceanography 5 (1), 1–13.
McGillicuddy, D.J., Sedwick, P.N., Dinniman, M.S., Arrigo, K.R., Bibby, T.S., Greenan, B. J.W., Hofmann, E.E., Klinck, J.M., Smith Jr., W.O., Mack, S.L., Marsay, C.M., Sohst, B.M., van Dijken, G.L., 2015. Iron supply and demand in an Antarctic shelf ecosystem. J. Geophys. Res. 42 (19), 8088–8097.
Mengesha, S., Dehairs, F., Fiala, M., Elskens, M., Goeyens, L., 1998. Seasonal variation of phytoplankton community structure and nitrogen uptake regime in the Indian Sector of the Southern Ocean. Polar Biol. 20 (4), 259–272.
Michels, J., Dieckmann, G.S., Thomas, D.N., Schnack-Schiel, S.B., Krell, A., Assmy, P., Kennedy, H., Papadimitriou, S., Cisewski, B., 2008. Short-term biogenic particle flux

under late spring sea ice in the western Weddell Sea. Deep-Sea Res. II 55, 1024–1039.
Mishonov, A.V., Gardner, W.D., Richardson, M.J., 2003. Remote sensing and surface POC concentration in the South Atlantic. Deep-Sea Res. II 50, 2997–3015.
Mitchell, B.G., Brody, E.A., Holm-Hansen, O., McClain, C., Bishop, J., 1991. Light limitation of phytoplankton biomass and macronutrient utilization in the Southern Ocean. Limnol. Oceanogr. 36, 1662–1677.
Mongin, M., 2010Australian Antarctic Data Centre (Ed.), CTD Niskin Data Collected from the BROKE-West Voyage of the Aurora Australis, Ver. 1. Australian Antarctic Data Centre. https://doi.org/10.4225/15/598802b56c6d1.
Montes-Hugo, M., Doney, S.C., Ducklow, H.W., Fraser, W., Martinson, D., Stammerjohn, S.E., Schofield, O., 2009. Recent changes in phytoplankton communities associated with rapid regional climate change along the Western Antarctic Peninsula. Science 232 (5920), 1470–1473.
Morán, X.A.G., López-Urrutia, Á., Calvo-Díaz, A., Li, W.K.W., 2010. Increasing importance of small phytoplankton in a warmer ocean. Global Change Biol. 16 (3), 1137–1144.
Moreau, S., di Fiori, E., Schloss, I.R., Almandoz, G.O., Esteves, J.L., Paparazzo, F.E., Ferreyra, G.A., 2013. Deep-Sea Res. Part I Oceanogr. Res. Pap. 82, 59, 44s.
Moreau, S., D, L., J, J., Arroyo, M., Corkill, M., Cougnon, E., Genovese, C., Legresy, B., Lenton, A., Puigcorbé, V., Ratnarajah, L., Rintoul, S.R., Roca-Martí, M., Rosenberg, M., Shadwick, E.H., Silvano, A., Strutton, P.G., Tilbrook, B., 2019. sea ice meltwater and circumpolar deep water drive contrasting productivity in three antarctic polynyas. J. Geophys. Res.: Oceans 124 (5), 2943–2968.
Moreau, S., Boyd, P.W., Strutton, P.G., 2020. Remote assessment of the fate of phytoplankton in the Southern Ocean sea-ice zone. Nat. Commun. 11, 3108.
Nemirovskaya, I.A., Chemyavskii, N.G., 2011. (Table 2b) Concentration of Organic Compounds in Slush and Under-ice Water of the Southeast Sector of the Antarctic in March-April 2008. PANGAEA. https://doi.org/10.1594/PANGAEA.769948.
Nemirovskaya, I.A., E Artem'ev, V., 2013. (Table 2a) Concentration of Particulate Matter and Organic Compounds in Ice and Water of the Lazarev and Cooperation Seas. P.P. Shirshov Institute of Oceanology, Russian Academy of Sciences, Moscow, PANGAEA. https://doi.org/10.1594/PANGAEA.816669.
Nodder, S.D., Waite, A.M., 2003. Particulate Organic Carbon Flux of Trap T7-9_J from the Iron-Fertilized Area of SOIREE. PANGAEA. https://doi.org/10.1594/PANGAEA.107674.
Obernosterer, I., Fourquez, M., Blain, S., 2015. Fe and C co-limitation of heterotrophic bacteria in the naturally fertilized region off the Kerguelen Islands. Biogeosciences 12 (6), 1983–1992.
Owens, N.P.J., Priddle, J., Whitehouse, M.J., 1991. Variations in phytoplanktonic nitrogen assimilation around south Georgia and the bransfield strait (Southern Ocean). Mar. Chem. 35, 287–304.
Owens, S.A., Buesseler, K.O., Sims, K.W.W., 2011. Re-evaluating the $^{238}$sU-salinity relationship in seawater: implications for the $^{238}$U-$^{234}$Th disequilibrium method. Mar. Chem. 127, 31–39.
Owens, S.A., Pike, S., Buesseler, K.O., 2015. Thorium-234 as a tracer of particle dynamics and upper ocean export in the Atlantic Ocean. Deep Sea Res. Part II Top. Stud. Oceanogr. 116, 42–59.
Pasquer, B., Mongin, M., Johnston, N., Wright, S., 2010. Distribution of particulate organic matter (POM) in the Southern Ocean during BROKE-West (30°E - 80°E). Deep Sea Res, II: Topic. Stud. Oceanogr. 57 (9–10), 779–793.
Passow, U., Carlson, C.A., 2012. The biological pump in a high CO2 world. Mar. Ecol. Prog. Ser. 470, 249–271.
Passow, U., Alldredge, A.L., Logan, B.E., 1994. The role of particulate carbohydrate exudates in the flocculation of diatom blooms. Deep Sea Res. I: Oceanogr. Res. Pap. 41, 335–357.
Puigcorbé, V., Roca-Martí, M., Masque, P., Benitez-Nelson, C.R., Loeff, M. Rutgers v. d., Laglera, L.M., Bracher, A., Cheah, W., Strass, V.H., Hoppema, M., Santos-Echeandia, J., P, B., Hunt, V., Pakhomov, E.A., Klaas, C., 2017a. Particulate organic carbon export across the antarctic circumpolar current at 10°E: differences between north and south of the antarctic polar. Front. Deep Sea Res. Part II: Topic. Stud. Oceanogr. 138, 86–101.
Puigcorbé, V., Roca-Martí, M., Masque, P., Benitez-Nelson, C.R., Loeff, M. Rutgers v. d., Bracher, L.A., Moreau, S., 2017b. Latitudinal distributions of particulate carbon export across the north western atlantic ocean. Deep-Sea Res. Part I Oceanogr. Res. Pap. 129 (116), 130.
Puigcorbé, V., Masqué, P., Le Moigne, F.A.C., 2020. Global database of ratios of particulate organic carbon to thorium-234 in the ocean: improving estimates of the biological carbon pump. Earth Syst. Sci. Data 12, 1267–1285.
R Core Team, 2014. R: A Language and Environment for Statistical Computing. R Foundation for Statistical Computing, Vienna, Austria. ISBN 3-900051-07-0. http://www.R-project.org/.
Ratnarajah, L., Nicol, S., Bowie, A.R., 2018. Pelagic iron recycling in the Southern Ocean: exploring the contribution of marine animals. Front. Mar. Sci. 5 (109).
Rembauville, M., Blain, S., Armand, L., Quéguiner, B., Salter, I., 2015. Export fluxes in a naturally iron-fertilized area of the Southern Ocean – Part 2: importance of diatom resting spores and faecal pellets for export. Biogeosciences 12, 3171–3195.
Rembauville, M., Briggs, N., Ardyna, M., Uitz, J., Catala, P., Penkerc'h, C., Poteau, A., Claustre, H., Blain, S., 2017. Plankton assemblage estimated with BGC-argo floats in the Southern Ocean: implications for seasonal successions and particle export. J. Geophys. Res.: Oceans 122, 8278–8292.
Roca-Martí, M., Puigcorbé, V., Iversen, M.H., Rutgers van der Loeff, M., Klaas, C., Cheah, W., Bracher, A., Masqué, P., 2017. High particulate organic carbon export during the decline of a vast diatom bloom in the Atlantic sector of the Southern Ocean. Deep Sea Res, II: Topic. Stud. Oceanogr. 138, 102–115.
Romankevich, E.A., Peresypkin, V.I., 1994. Table 1) Concentrations of Particulate Organic Carbon in the South Atlantic in February-March 1989. PANGAEA. https://doi.org/10.1594/PANGAEA.761073.
Romero, O., Armand, L.K., 2010. Marine Diatoms as Indicators of Modern Changes in Oceanographic Conditions. Cambridge University Press.
Rosenberg, M., Rintoul, S., 2017. Aurora Australis marine science cruise AU1602, Dalton, Mertz and Ninnis CTDs - oceanographic field measurements and analysis. https://researchdata.ands.org.au/aurora-australis-marine-measurements-analysis/1358680?fl.
Rutgers van der Loeff, M.M., 2007. Manual determination of Thorium 234 and Uranium 238 in surface water during cruise ANT-XXIII/3. https://doi.org/10.1594/PANGAEA.615832.
Sedwick, P.N., Di Tullio, G.R., 1997. Regulation of algal blooms in Antarctic shelf waters by the release of iron from melting sea ice. Geophys. Res. Lett. 24, 2515–2518.
Sedwick, P.N., Bowie, A.R., Trull, T.W., 2008. Dissolved iron in the Australian sector of the Southern Ocean (CLIVAR SR3 section): meridional and seasonal trends. Deep Sea Res. Oceanogr. Res. Pap. 55 (8), 911–925.
Shadwick, E.H., Tilbrook, B., Williams, G.D., 2014. Carbonate chemistry in the Mertz Polynya (East Antarctica): biological and physical modification of dense water outflows and the export of anthropogenic $CO_2$. J. Geophys. Res.: Oceans 119, 1–14.
Silvano, A., Rintoul, S.R., Peña-Molino, B., Williams, G.D., 2017. Distribution of water masses and meltwater on the continental shelf near the Totten and Moscow University ice shelves. J. Geophys. Res.: Oceans 122, 2050–2068.
Smetacek, V., Klaas, C., Strass, V.H., Assmy, P., Montresor, M., Cisewski, B., Savoye, N., Webb, D.J., d'Ovidio, F., Arrieta, J.M., Bathmann, U., Bellerby, R., Berg, G.M., Croot, P., Gonzalez, S., Henjes, J., Herndl, G.J., Hoffmann, L.J., Leach, H., Losch, M., Mills, M.M., Neill, C., Peeken, I., Röttgers, R., Sachs, O., Sauter, E., Schmidt, M.M., Schwarz, J., Terbrüggen, A., Wolf-Gladrow, D.A., 2012. Deep carbon export from a Southern Ocean iron-fertilized diatom bloom. Nature 487 (313), 1–26.
Stange, P., Bach, L.T., C Le Moigne, F.A., Taucher, J., Boxhammer, T., Riebesell, U., 2017. Quantifying the time lag between organic matter production and export in the surface ocean: implications for estimates of export efficiency. Geophys. Res. Lett. 44 (1), 268–276.
Steinberg, D.K., Landry, M.R., 2017. Zooplankton and the ocean carbon cycle. Ann. Rev. Mar. Sci 9, 413–444.
Sterner, R.W., Elser, J.J., 2002. Ecological Stoichiometry: the Biology of Elements from Molecules to the Biosphere, first ed. Princeton Univ. Press.
Stramski, D., Reynolds, R., Babin, M., Kaczmarek, S., Lewis, M.R., Röttgers, R., Sciandra, A., Stramska, M., Twardowski, M.S., Franz, B.A., Claustre, H., 2008. Relationships between the surface concentration of particulate organic carbon and optical properties in the eastern South Pacific and eastern Atlantic Oceans. Biogeosciences 5, 171–201.
Strzepek, R., Hunter, K., Frew, R., Harrison, P., Boyd, P., 2012. Iron-light interactions differ in Southern Ocean phytoplankton. Limnol. Oceanogr. 57, 1182–1200.
Thomalla, S., Ogunkoya, A., Vichi, M., Swart, S., 2017. Using optical sensors on gliders to estimate phytoplankton carbon concentrations and chlorophyll-to-carbon ratios in the Southern Ocean. Front. Mar. Sci. 4, 34.
Thomson, R.E., Fine, I.V., 2003. Estimating mixed layer depth from oceanic profile data. J. Atmos. Ocean. Technol. 20, 319–329.
Tréguer, P., Bowler, C., Moriceau, B., Dutkiewicz, S., Gehlen, M., Aumont, O., Bittner, L., Dugdale, R., Finkel, Z., Ludicone, D., Jahn, O., Guidi, L., Lasbleiz, M., Leblanc, K., Levy, M., Pondaven, P., 2017. Influence of diatom diversity on the ocean biological carbon pump. Nat. Geosci. 11, 27–37.
Trull, T.W., Armand, L.K., 2013. $\delta^{13}$C Content of Organic Carbon Measured on Pumped Water Samples during TANGAROA Cruise SOIREE. PANGAEA. https://doi.org/10.1594/PANGAEA.807878.
Turley, C.M., Mackie, P.J., 1994. Biogeochemical significance of attached and free-living bacteria and the flux of particles in the NE Atlantic Ocean. Mar. Ecol. Prog. Ser. 115, 191–203.
Turner, J.T., 2015. Zooplankton fecal pellets, marine snow, phytodetritus and the ocean's biological pump. Prog. Oceanogr. 130, 205–248.
Usbeck, R., Rutgers van der Loeff, M., Hoppema, M., Schlitzer, R., 2002. Shallow remineralization in the weddell gyre. G-cubed 3 (1), 1–18.
Yager, P.L., Sherrell, R.M., Stammerjohn, S.E., Ducklow, H.W., Schofield, O.M.E., Ingall, E.D., Wilson, S.E., Lowry, K.E., Williams, C.M., Riemann, L., Bertilsson, S., Alderkamp, A.C., Dinasquet, J., Logares, R., Richert, I., Sipler, R.E., Melara, A.J., Mu, L., Newstead, R.G., Post, A.F., Swalethorp, R., van Dijken, G.L., 2016. A carbon budget for the Amundsen Sea Polynya, Antarctica: estimating net community production and export in a highly productive polar ecosystem. Elementa: Sci. Anthropocene 1–37.